ICARUS 89, 168–189 (1990)

The Spectrum of Saturn from 1990 to 2230 cm^{-1}: Abundances of AsH_3, CH_3D, CO, GeH_4, NH_3, and PH_3

KEITH S. NOLL[1] AND HAROLD P. LARSON[2]

Lunar and Planetary Laboratory, University of Arizona, Tucson, Arizona 85721

Received March 23, 1990; revised July 31, 1990

We have investigated the mole fractions of six gases (AsH_3, CH_3D, CO, GeH_4, NH_3, and PH_3) from extensive computer modeling of a high-resolution spectrum of Saturn from 1994 to 2229 cm^{-1} (4.5 to 5.0 μm). Five new AsH_3 spectral features and three previously observed absorptions were detected, leaving no doubt as to the presence of this gas in Saturn. The mole fraction of AsH_3 is $\sim 3 \times 10^{-9}$, in agreement with earlier work and 10 times higher than that found in Jupiter. Thirteen lines of CO were detected, including eight new lines. Our CO abundance is lower than previous estimates, which we attribute to an improved atmospheric model. We find that the CO mole fraction is 1×10^{-9} if its distribution is uniform and 2.5×10^{-8} if concentrated in the stratosphere at pressures $P < 80$ mbar. The detection of one high-J line of CO in Saturn's spectrum, $P14$, favors a tropospheric distribution but the evidence is not strong enough to make a firm conclusion regarding the vertical distribution of CO. The PH_3 abundance increases dramatically below the photochemically active portion of the atmosphere. For $P < 400$ mbar the PH_3 mole fraction was fixed at 1×10^{-6}, in agreement with previous work, which produced a good fit to that region of Saturn's 5-μm spectrum dominated by reflected sunlight. At $P > 400$ mbar, however, we find that the PH_3 mole fraction is $7^{+3}_{-2} \times 10^{-6}$, which indicates a surprisingly high elemental abundance of P in Saturn. The mole fraction of CH_3D is $(3.3 \pm 1.5) \times 10^{-7}$, in general agreement with values determined at other wavelengths, which leads to a D/H ratio of $(1.7 \pm 1.1) \times 10^{-5}$. Our constraints to the abundances of GeH_4 and NH_3 are weak. We find that the mole fraction of GeH_4 is $(4 \pm 4) \times 10^{-10}$ and that of NH_3 is $\leq 3 \times 10^{-4}$. The observed elemental abundances of P and As are important as remnants of the solid component of the solar nebula. Their pattern of enrichment in Jupiter and Saturn appears to be different than that for C and N.

1. INTRODUCTION

The elemental compositions of the giant planets inferred from spectrochemical analyses of their atmospheric constituents are fundamental data in solar system science. Complete inventories of the elemental abundances in each planet and, especially, the ability to compare one set to another promise great insight into understanding the processes that formed the outer planets and the solar system as a whole. In spite of the lack of *in situ* measurements, much progress has been made in addressing the interrelated problems of atmospheric composition, thermal profiles, cloud structure, radiative transfer, and vertical inhomogeneity through the interpretation of remotely observed spectra from ultraviolet to radio wavelengths. The 5-μm spectral region has been particularly informative because of a narrow window ($\sim$1800–2300 cm^{-1}) of low opacity in both the Earth's and the outer planets' atmospheres through which remote observations probe to deeper levels than is possible at all but radio wavelengths. This spectral region contains the fundamental bands of numerous gaseous hydrides whose presence as trace constituents in planetary atmospheres provides important clues to their origin and evolution. The importance of the 5-μm spectral region may be gauged from the fact that seven of the eight known elements in Saturn and Jupiter and the hydrogen isotope deuterium are found in molecules that contribute to their 5-μm spectra. This premier hunting ground for new molecules has led to the discovery of three of the eight known elements (O, Ge, and As) in Saturn in just the last 4 years. The spectroscopic observations of Saturn at 5 μm are summarized in Table I.

In the first published spectrum, Fink and Larson (1978) detected multiple features of the ν_2 band of monodeuterated methane (CH_3D) from which they estimated Saturn's D/H ratio to be $\sim 2 \times 10^{-5}$, similar to Jupiter's value but less than the terrestrial value (1.5×10^{-4}). The first complete spectrum of Saturn's 5-μm window was ac-

[1] Present address: Code ES-63, NASA Marshall Space Flight Center, Huntsville, AL 35812.

[2] Visiting Astronomer, Infrared Telescope Facility, operated by the University of Hawaii under contract from the National Aeronautics and Space Administration.

0019-1035/90 $3.00

TABLE I
Observations of Saturn at 5 μm

Reference	Molecule analyzed	Spectral resolution (cm^{-1})	Spectral bandpass (cm^{-1})	Instrument	Facility
Fink and Larson 1978	CH_3D	2.8	2000–3000	FTS	UAO
Larson *et al.* 1980	PH_3	2.0	1800–2699	FTS	UAO
Fink *et al.* 1983	NH_3	1.2	1800–2000	FTS	IRTF
Courtin *et al.* 1984	NH_3	4.3	1880–1960	FTS	Voyager
Noll *et al.* 1986	CO	0.15	2157–2159 2154–2156 2139–2142 2131–2133 2123–2125 2081–2083	FP	UKIRT
Noll *et al.* 1988a	GeH_4	0.15	2154–2156 2149–2152 2139–2142 2133–2136 2082–2085	FP	UKIRT
Noll *et al.* 1989	AsH_3	0.25	2109–2130	FP	UKIRT
Bézard *et al.* 1989	AsH_3	0.10	2090–2170	FTS	CFHT
This work	AsH_3, CH_3D, CO, GeH_4, NH_3, PH_3	0.28	1990–2230	FTS	IRTF

quired by Larson *et al.* (1980) who confirmed the presence of phosphine (PH_3) in Saturn and demonstrated that this trace constituent dominates the shape of Saturn's 5-μm spectrum, a condition that would impede quantitative spectral analyses for many years because the spectrum of PH_3 itself was not understood. Fink *et al.* (1983) found evidence for a subsolar abundance of NH_3 and they determined that Saturn's flux from 5.0 to 5.4 μm was mostly thermal in origin with some contribution from reflected solar radiation. Courtin *et al.* (1984) also concluded that the tropospheric abundance of NH_3 (P = 2 bars) was low, approximately half the solar value, from an average of 3357 individual Voyager 1 IRIS spectra. Noll *et al.* (1986, 1988a, 1989) and Noll (1987) conducted a series of observations of Saturn at resolution limits up to 0.13 cm^{-1}, less than the natural width (~0.2 cm^{-1}) of the planetary lines. Their observations represented an order-of-magnitude improvement in resolution over previous work, but only in relatively narrow spectral passbands because of the bandwidth limitation of Fabry–Perot spectrometers. These spectra established the presence of CO, GeH_4, and AsH_3 in Saturn and provided evidence for a PH_3 abundance higher than previous measurements. Bézard *et al.* (1987, 1988, 1989) and Drossart *et al.* (1987) used the latest results from laboratory spectral analyses to interpret their IR observations of Saturn. Their contributions included independent detections of GeH_4 and AsH_3, confirmation of the presence of CO, and strong evidence for a superabundance of PH_3.

In general, the development of observational and interpretive capabilities for Saturn at 5 μm followed successful and often surprising results from 5-μm studies of Jupiter. Compared to Jupiter, however, Saturn presented several difficulties that usually delayed progress in acquiring and interpreting data. One natural constraint is Saturn's intrinsically lower flux due both to its more distant location from the Sun and to its lower brightness temperature (T_b ~200°K for Saturn, ~270°K for Jupiter's "hot spots"). Observations have therefore depended entirely on the use of Fourier transform (FTS) and Fabry–Perot (FP) spectrometers at optimized IR facilities (see Table I) to provide high optical efficiency at high spectral resolution with minimum interference from telluric absorption and thermal background radiation. A second natural complication is the transition from reflected solar flux to thermal emission that occurs across Saturn's 5-μm spectrum, a situation that requires a much more complicated atmospheric model for quantitative spectral analyses. Finally, the unexpected detection of certain trace constituents (e.g., PH_3, AsH_3, GeH_4) in Jupiter and Saturn meant that laboratory analyses of their molecular band parameters were inadequate or unavailable for immediate use in the interpretation of planetary spectra.

We present in this paper an analysis of the abundance and vertical distribution of all known absorbers in Saturn's 5-μm spectrum. The key components of this project are previously unpublished observations of Saturn at 5 μm, synthetic spectra of each atmospheric constituent,

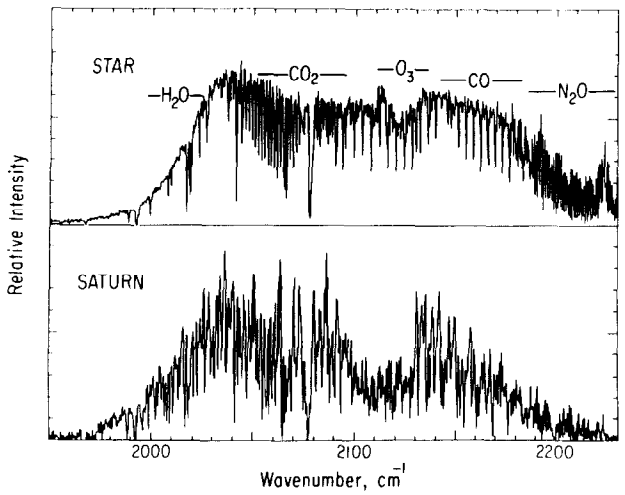

FIG. 1. Upper panel: Stellar comparison spectrum. Lower panel: The observed spectrum of Saturn. The achieved resolution in each spectrum is 0.28 cm^{-1}. The upper bound to these spectra at 1950 cm^{-1} is due to optical filtering; the lower limit at ~2250 cm^{-1} in Saturn is due to PH_3. The rms noise level is constant across each spectrum and is most clearly seen in the region of no signal below ~1970 cm^{-1}.

and an atmospheric model for synthesizing Saturn's spectrum for comparison with the observations. The observations combine high spectral resolution (0.28 cm^{-1}), only slightly larger than the intrinsic width of lines formed at P = 2–3 bars in Saturn's atmosphere, with a sufficiently wide spectral bandwidth to include spectral lines from all six molecules (see list in Table I) that contribute to Saturn's 5-μm spectrum. The model on which the calculations are based includes the abundances of all gaseous absorbers, their vertical distributions, clouds, and thermal and reflected solar components of planetary flux. By using this approach to reproduce the observations we achieved a coherent understanding not only of the many variables that affect Saturn's 5-μm spectrum, but also of similarities and differences between Jupiter and Saturn that relate to their origin and evolution (see Section 6).

2. OBSERVATIONS

The observed spectra (see Fig. 1) were acquired at the NASA Infrared Telescope Facility (IRTF) during 1981 March 28–31 with the University of Arizona FTS (Larson and Fink 1975). The achieved spectral resolution was 0.28 cm^{-1} (unapodized) and the instrumental field-of-view was 10 arcsec. The spectral bandpass was shaped by a cold short-pass interference filter with cut-on wavelength at 5.1 μm. This allowed observation of half of Saturn's 5-μm atmospheric transmission window at the maximum resolution possible with this FTS. Companion observations of the long wavelength portion of this window at lower spectral resolution were reported elsewhere (Fink *et al.* 1983). Instrumental and atmospheric transmission factors were determined from observations of comparison stars (α Aur, α CMi). Multiple observations of these stars at different airmasses allowed calculation of a weighted stellar comparison spectrum that matched the average airmass (1.2) in Saturn's spectrum. The absorption lines in the stellar average in Fig. 1 are due to telluric species. These interfering lines were eliminated from Saturn's spectrum by ratio techniques. The ratio spectrum was not calculated when transmission in the stellar spectrum was less than 10% of maximum, thus excluding frequencies <1994 cm^{-1} and >2229 cm^{-1}. Within this bandwidth there are several terrestrial absorption features that are strong enough to cause dropouts, such as the CO_2 Q branch at 2077 cm^{-1}. The many dropouts above 2200 cm^{-1} limit the usefulness of that portion of Saturn's spectrum. The absolute flux calibration of our spectrum of Saturn was transferred from a calibrated spectrum of Saturn at 1.8 cm^{-1} resolution that was recorded by Noll and Geballe (unpublished data) at the United Kingdom Infrared Telescope (UKIRT). The two spectra agreed well in their overlap region from 1994 to 2010 cm^{-1} when the higher-resolution IRTF spectrum was convolved with a Lorentz function to match the resolution of the UKIRT scan.

3. THE BASELINE MODEL

Spectrum synthesis is the primary tool used to understand a complex spectrum such as Saturn's in Fig. 1. Since its spectrum is the superposition of thousands of lines, very limited interpretation is possible from inspection of the spectrum itself or upon comparison with room temperature laboratory spectra. The recent detections of AsH_3 in Jupiter and Saturn emphasize this point. The AsH_3 Q branch at 2126 cm^{-1} (see Fig. 3) is a prominent feature, τ ~0.6 with width ~2.5 cm^{-1}, that could have been detected in the lower-resolution spectra of Saturn that were available a decade ago were it not for the lack of laboratory spectral analyses of the principal absorber in Saturn's 5-μm spectral window (PH_3) that made it impossible to interpret this region of Saturn's spectrum. By chance, the AsH_3 Q branch is surrounded by strong PH_3 absorption lines so that it does not form a prominent spectral "stalactite" in the continuum that could be identified by simple inspection, as was the case for GeH_4 in Jupiter (Fink and Larson 1978; see also Fig. 16). Instead, the presence of AsH_3 in Saturn was inferred only when a synthetic spectrum lacking AsH_3 revealed a spectral "stalagmite" upon comparison with the observations, thus indicating the presence of an unsuspected new absorber (see Fig. 1 in Noll *et al.* 1989).

The model that we present here represents a significant improvement over earlier efforts because of the quality of

its input data and its realistic treatment of the thermal structure of Saturn's atmosphere. Our approach makes optimum use of the high information content of the observations and the low-temperature laboratory studies of all relevant gaseous absorbers. In addition, we benefit from the insight gained from previous studies of Saturn at ground-based, airborne, and spacecraft facilities. This combination of inputs allows us to make more critical evaluations of Saturn's atmospheric parameters. The model has its limits, such as the simplistic manner in which clouds are introduced, but overall we believe that this comprehensive treatment of Saturn's 5-μm spectrum is an important advance in understanding the composition, structure, and evolution of its atmosphere.

The radiative transfer program used to generate the synthetic spectra is described in detail in Noll (1987). While straightforward in principle, several complicating factors arise in practice, such as the large amount of computer time required to generate a single comparison spectrum. Our strategy for calculating the large number of spectra required for this analysis was to fix as many of the model's parameters as possible with results from other studies, including the pressure–temperature structure of the atmosphere, the location, albedo, and thickness of cloud layers, and the abundance as a function of altitude of each of six molecular line absorbers. We calculated a preliminary series of spectra at very low resolution from which we selected parameters to define a baseline model that we adopted as a first-order fit to the observations. The generally good agreement between this baseline model and Saturn's observed spectrum is evident in Fig. 2. We then varied the abundances of individual molecules in the baseline model to improve the fit, a procedure used by Bjoraker *et al.* (1986a) for a similar analysis of Jupiter's 5-μm spectrum. Another complication is that knowledge of the vertical distribution of molecules is more important in Saturn than in Jupiter. Saturn's 5-μm flux is a combination of thermal radiation from a pressure level of several bars and reflected solar flux from a pressure level of a few hundred millibars where photodissociation of some molecules becomes important. The formation of a spectral line in Saturn's 5-μm spectrum is therefore sensitive to the abundance of a given species in both of these pressure regimes, whereas Jupiter's entire 5-μm spectrum is dominated by absorption in the region 2–7 bars, well below the photoreactive portion of the atmosphere.

A note on nomenclature is necessary. *Abundance* as used in this paper is a generic term indicating any one of several ways to quantify the amount of a particular molecule in an atmosphere. In the literature one finds *column abundance* (in units of molecules cm^{-2}, cm-amagat, cm-atm, and precipitable cm to name just a few),

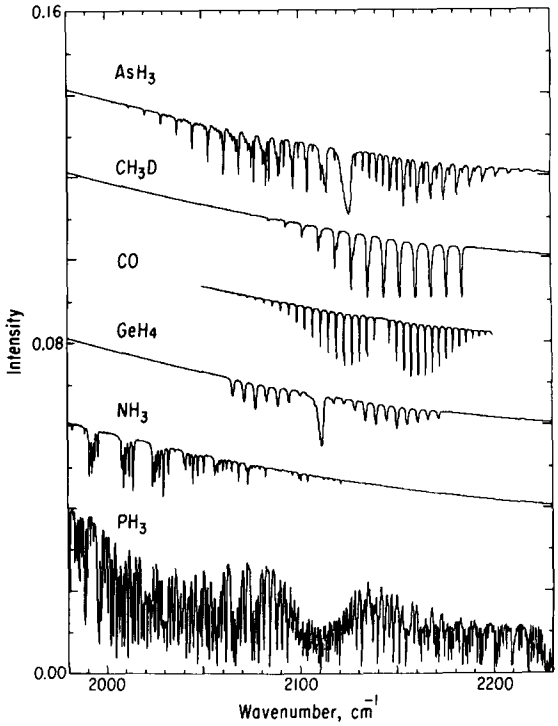

FIG. 3. Spectra of six molecules whose features contribute to Saturn's 5-μm spectrum. Each spectrum was synthesized using Saturn's P–T profile and the abundance adopted for the baseline compositional model. Their composite spectrum in Fig. 2 (upper panel) is the sum of the optical depths in these individual spectra. The similarity between the spectrum of PH_3 alone and Saturn's observed spectrum in Fig. 2 (lower panel) demonstrates the necessity of understanding its spectrum before attempting quantitative analyses of other constituents in this wavelength region.

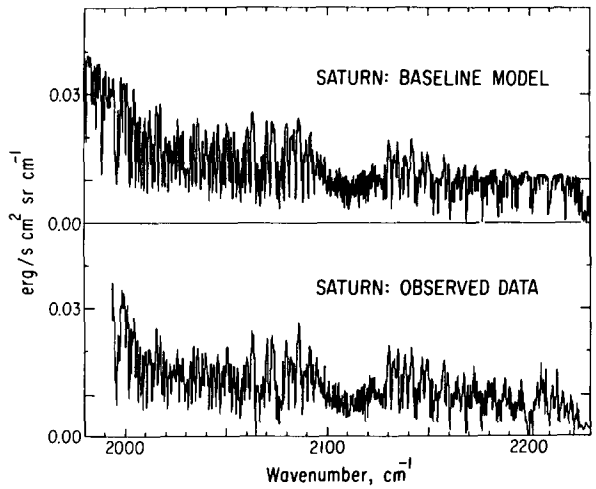

FIG. 2. Upper panel: Synthetic spectrum of Saturn at 5 μm calculated with the baseline compositional model. Lower panel: The calibrated spectrum of Saturn. Telluric absorptions were removed from Saturn's spectrum with ratio techniques. The similarities in the calculated and observed spectra are due to the spectral features of six gaseous constituents in Saturn's atmosphere.

mixing ratio (the number density of a molecule relative to that of H_2), and *mole fraction* (equal to the partial pressure of a molecule divided by the total atmospheric pressure). We will use *mole fraction*, denoted by q, for all abundance determinations in our analysis of Saturn's spectrum. To convert from *mole fraction* to *mixing ratio* divide by 0.96, the mole fraction of H_2 in Saturn (Conrath *et al.* 1984).

3.1. Laboratory Spectroscopy

Spectral line information (line positions, line strengths, lower-state energy levels, and pressure broadening coefficients) now exists for nearly all of the lines within Saturn's 5-μm spectrum. A synthetic spectrum of each of the molecules included in our atmospheric model is displayed separately in Fig. 3. Each spectrum was computed for the conditions of pressure, temperature, abundance, and distribution in Saturn's baseline model.

It is apparent from Fig. 3 that the complex spectrum of PH_3 dominates this region of Saturn's 5-μm spectrum and that quantitative analysis of any atmospheric constituent is impossible until the spectrum of PH_3 itself can be simulated for conditions appropriate to planetary atmospheres. Tarrago *et al.* (1987) compiled a line list for the $2\nu_2$ and $\nu_2 + \nu_4$ bands of PH_3 centered, respectively, at 1972 cm^{-1} and in the broad feature from 2090 to 2130 cm^{-1}. The ν_1 and ν_3 bands of PH_3, which absorb at frequencies above 2180 cm^{-1}, are listed in the GEISA molecular line list (Chedin *et al.* 1986). Uncertainties in the PH_3 line strengths can significantly affect spectrochemical analyses of other molecules that contribute to the spectrum. In particular, the generally higher uncertainty that usually applies to the strengths of high-J lines may be partially responsible for the difficulties that we encountered in fitting the region 2000–2050 cm^{-1} of Saturn's spectrum (see Section 4.6). Unfortunately, uncertainties in the PH_3 lines have not been published, so we can only speculate about their consequences.

Lellouch *et al.* (1987) constructed a line list for NH_3 near 5 μm based on low-temperature data. Similar information for AsH_3 was prepared by Tarrago *et al.* (Bézard, private communication) using, in part, spectra of AsH_3 from Larson (unpublished data). Bézard *et al.* (1989) indicated that the uncertainty in the AsH_3 line strengths is ±30%. Pressure broadening coefficients for PH_3, NH_3, and AsH_3 have not been measured. The authors have somewhat arbitrarily set them at 0.071 cm^{-1} atm^{-1} for the $2\nu_2$ and $\nu_2 + \nu_4$ bands of PH_3, 0.075 cm^{-1} atm^{-1} for the ν_1 and ν_3 bands of PH_3, 0.076 cm^{-1} atm^{-1} for NH_3, and 0.080 cm^{-1} atm^{-1} for AsH_3. The arbitrary nature of these widths does not affect our results. Measured pressure broadening coefficients typically range between 0.05 and 0.10 cm^{-1} atm^{-1} so for a maximum atmospheric pressure of ~3 bars and a spectral resolution of 0.28 cm^{-1}, factor of 2 variations in pressure broadening coefficients would be difficult to discern in the analysis.

Carbon monoxide is the best studied gaseous constituent in Saturn's 5-μm spectrum because it is often used as a frequency and intensity standard. Molecular parameters for CO are available in either the GEISA (Chedin *et al.* 1986) or the AFGL (Rothman *et al.* 1983) molecular line compilations and the CO–H_2 pressure broadening coefficients are in Draegert and Williams (1968).

Deuterated methane was studied by Chackerian and Guelachvili (1983) who gave line positions and strengths for the ν_2 band. A pressure broadening coefficient of 0.075 cm^{-1} atm^{-1} was assumed, slightly higher than the coefficient found for two CH_3D lines studied by Chudamani and Varanasi (1987). Unfortunately, Chackerian and Guelachvili's list did not include the Q branch at 2199 cm^{-1} nor the P1 line at 2192 cm^{-1} because of saturation effects at the high abundances used in the experiment (Chackerian, private communication). These missing features show up later in our analysis, but they do not affect our retrieved CH_3D abundance because many other CH_3D lines are available in the observations.

The GeH_4 spectrum in Fig. 3 represents a compilation of data for all five isotopes from several sources (Giver and Chackerian 1990; Varanasi and Chudamani 1987; Robiette, private communication, see Noll *et al.* 1988a for details). The absence of high-J lines is not an impediment because even the strongest low-J GeH_4 lines are barely detectable in Saturn's spectrum.

3.2. Pressure–Temperature Profile

The P–T profile used in this work (see Fig. 4) is the Voyager 2 Radio Science ingress profile presented by Courtin *et al.* (1984). We assume that the thermal profile follows an adiabat with lapse rate of 0.9 K km^{-1} below P = 1 bar and T = 137°K. Variations in the thermal profile could have small effects on our retrieved molecular abundances, but we considered them negligible relative to other uncertainties in the model and the molecular line parameters.

3.3. Clouds and the Balance of Thermal and Reflected Radiation

We assume a two-cloud model similar to that in Tomasko *et al.* (1984, see their Fig. 15) and displayed schematically in Fig. 4. The upper cloud is assumed to be relatively optically thin at 5 μm ($\tau_5 < 1$); in our model 75% of the radiation from below passes through it. The top of this cloud, which we use as the weak reflecting layer, is at P = 400 mbar and T = 103°K and it has a geometric albedo p_5 = 0.09 at 5 μm. The composition of this cloud is not addressed in this paper, although we note that some atmospheric models predict an NH_3 ice cloud at this loca-

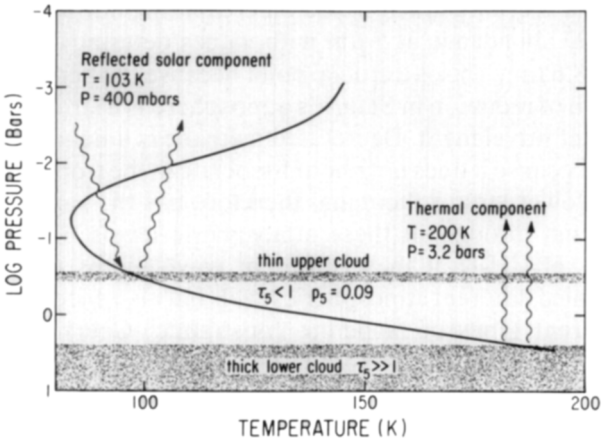

FIG. 4. The variation of atmospheric temperature with pressure in our model (solid curve) is based on the profile retrieved from the Voyager 2 RSS experiment. The pressure levels at which cloud layers exist in our model are indicated with the shaded areas. Two radiative processes contribute to Saturn's spectrum at 5 μm: reflection of solar flux from the upper cloud layer, and thermal emission from lower atmospheric levels.

tion and we refer to it as such in the remainder of the paper. The lower cloud in our model occurs at $T = 200$ K and $P = 3.2$ bars. This cloud is assumed to be optically thick ($\tau_5 \gg 1$) and, therefore, to form the effective bottom of the atmosphere. This lower cloud is at the location of the predicted NH_4SH cloud and again we use this possible composition as a convenient label. Both clouds emit as graybodies: the Planck function for their respective temperatures is multiplied by their assumed IR emissivities. The emissivity of the lower cloud is unity while the contribution from the upper cloud is entirely negligible for any assumed emissivity.

The relative contribution of the reflected and thermal components of Saturn's total flux is a strong function of frequency, as demonstrated in Fig. 5. The fraction of reflected solar radiation increases steadily with frequency as a result of the monotonic decline in blackbody thermal emission from the planet. Within this transition region there are very narrow *microwindows*, typically a few reciprocal centimeters wide such as between 2081 and 2084 cm^{-1}, where low molecular opacity causes the fraction of thermal radiation to increase. Within these narrow intervals of low gas opacity we sense the deepest levels of the atmosphere accessible in this wavelength region and consequently the greatest column abundance of gas. When absorption lines of minor atmospheric constituents happen to coincide with one of these microwindows we have maximum sensitivity to their abundance by virtue of the increased path length and reduced interference from nearby spectral lines.

The cloud parameters adopted above result from preliminary fits to our data, with heaviest emphasis on spectral regions that are dominated either by reflected sunlight (2110–2127 cm^{-1}, 2170–2229 cm^{-1}) or by thermal radiation (1990–2010 cm^{-1}). We characterized the reflected component in our baseline model by estimating the pressure and geometric albedo of the upper cloud as follows. The abundance of PH_3, the principal absorber in the stratosphere in this wavelength region, was set to the value derived from observations at 10 μm (see Section 3.4.1). We then calculated test spectra with the reflecting cloud located at pressures from 1000 to 100 mbar, with geometric albedos adjusted to match observed flux levels. Calculations with pressures from 300 to 500 mbar gave the best results so we chose $P = 400$ mbar for the baseline model.

In this preliminary phase we also varied the AsH_3 and GeH_4 mole fractions above the cloudtop and found acceptable fits for $q_{AsH_3} = 8 \times 10^{-11}$ and $q_{GeH_4} = 2 \times 10^{-10}$ in the interval 2110–2127 cm^{-1}, although the sensitivity to changes in these abundances was low. Abundances of AsH_3, GeH_4, and PH_3 above the reflecting cloud are expected to be lower than tropospheric values because of photodissociation by solar ultraviolet photons and energetic hydrogen atoms (Fegley 1988, Fegley and Prinn 1985, Prinn *et al.* 1984). Bézard *et al.* (1988) reported

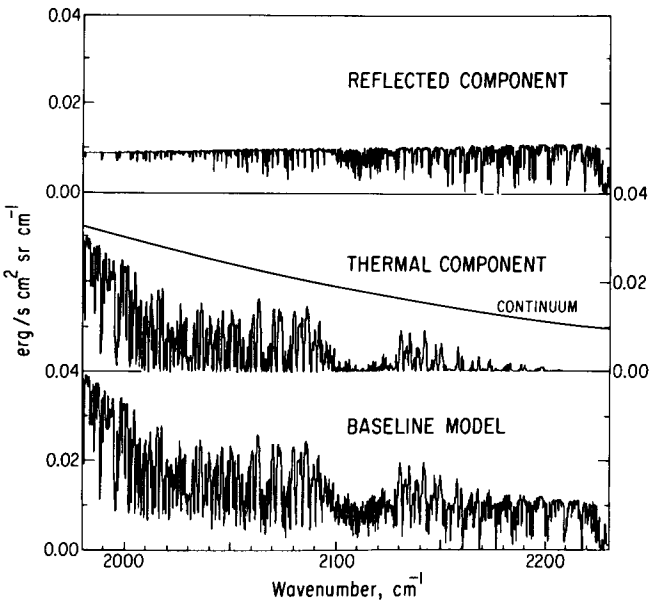

FIG. 5. Comparison of the two components of flux in Saturn's spectrum at 5 μm. Upper panel: Reflected solar component alone. Center panel: Thermal emission component alone. Lower panel: Superposition of both components in the baseline model. These synthetic spectra demonstrate that Saturn's observed spectrum at 5 μm is dominated by the reflected component at ~2200 cm^{-1} and by the thermal component at ~2000 cm^{-1}. The transition region includes the most diagnostic spectral features of four of Saturn's atmospheric constituents (see Fig. 3), hence the need for a comprehensive atmospheric model for their analyses.

evidence for a factor of 4 depletion of AsH_3 in the region 200–400 mbar compared to that found at deeper levels. Both Noll (1987) and Bézard *et al.* (1987) reported PH_3 abundances at $P > 1$ bar in Saturn's atmosphere that are higher than those found at 10 μm, where only the abundance above the cloudtops is sampled. Since we anticipated a similar result from our 5-μm analysis, we did not attempt to fine-tune the stratospheric abundances of these gases. It is the mole fraction of gas beneath the upper cloud and below any region of condensation or photodissociation that is most useful for inferring the elemental composition of a planetary atmosphere.

Having specified the reflected component in our model, we next estimated the temperature of the lower, NH_4SH cloud and the transmission of the upper, NH_3 cloud. The overall shape of the 5-μm continuum is weakly dependent on temperature for the range 180–210 K obtained from Voyager spectral analyses (Hanel *et al.* 1981). A rough visual impression of the continuum shape is provided by transmission peaks between spectral lines but the complex superposition of molecular lines in Saturn's 5-μm spectrum limits the usefulness of this approach, as can be seen by comparing the baseline model (lower panel in Fig. 5) with the thermal continuum alone (center panel in Fig. 5). The NH_4SH cloud temperature cannot be less than ~196°K because the outgoing flux would be too low even with no attenuation from the NH_3 cloud. It is more difficult to place an upper limit to the temperature of the NH_4SH cloud because of the possibility of distributed attenuation there and because the opacity of the overlying NH_3 cloud is unconstrained. Bézard *et al.* (1989) achieved an excellent fit to their data using a model with distributed opacity in the NH_4SH cloud. However, we preferred a simplified model in which the lower cloud is essentially an opaque blackbody because this approach reduces the number of free parameters. We preferred to think of the upper cloud as optically thin and weakly absorbing at these frequencies so that the transmission would be comparable to unity minus the geometric albedo. After many trials we chose a lower cloud temperature of 200°K and an upper cloud transmission of 75%.

The uncertainty associated with specification of the lower, NH_4SH cloud is a major source of error in converting our retrieved column abundances to mole fractions. Since the column abundance N scales as the pressure, $N = nH = (P/kT)(kT/mg)$, if the cloud were actually at $P = 4$ bars instead of 3.2 bars, for example, we would overestimate the mole fraction by as much as 25%. Pressures much greater than this are ruled out by the absence of the CH_4 "hot band" at 1932 cm^{-1} (Noll and Geballe, unpublished data), while lower pressures are not compatible with the observed brightness temperature.

An important issue which we address here is the credibility of the model. The principal test that we apply is an a posteriori argument based on comparing our measured CH_3D abundance at 5 μm with values determined at 1.6 and 8.6 μm. This is a crucial point because the penetration depth of radiation in Saturn's atmosphere is a strong function of wavelength. Deuterated methane is unique for this test because it does not photodissociate in the troposphere and lower stratosphere and therefore has the same mole fraction throughout these atmospheric levels. Observations of CH_3D at these different wavelengths not only sampled different atmospheric levels but also encountered different types of modeling constraints. Courtin *et al.* (1984) derived $CH_3D/H_2 = (3.9 \pm 2.5) \times 10^{-7}$ from Voyager data at 8.6 μm. Atmospheric sounding at these wavelengths is not as deep as at 5 μm because the pressure-induced opacity of H_2 becomes high at pressures of only a few hundred millibars. At 1.6 μm Owen *et al.* (1986) found $CH_3D/CH_4 = (6.8^{+6.8}_{-3.2}) \times 10^{-5}$ from which $CH_3D/H_2 = 3.2 \times 10^{-7}$ for $qCH_4 = 4.5 \times 10^{-3}$ (Courtin *et al.* 1984). In this spectral region the measured CH_3D abundance is more sensitive to modeling the haze and upper clouds of Saturn than at longer wavelengths. The CH_3D abundance that we find in Section 4.2, $qCH_3D = (3.3 \pm 1.5) \times 10^{-7}$ [corresponding to $CH_3D/H_2 = (3.4 \pm 1.6) \times 10^{-7}$] is within the range of these other two measurements even though the limiting uncertainties of the models were different. This consistency alone does not validate our model, but it does significantly increase our confidence in it.

The issue of uniqueness is more difficult to address. By fixing the cloud parameters as described above, we selected just one of a range of possibilities. Our choice is reasonable given the available constraints, but other constructions are possible (see, e.g., Bézard *et al.* 1989). The real issue is the extent to which these choices affect the derived mole fractions. We estimated that the most critical parameter, the location of the lower cloud, may introduce errors as large as 25% in measured mole fractions. Other free parameters such as the P–T profile and the upper cloud albedo have smaller effects on the molecular abundances.

3.4. Molecular Abundances in the Baseline Model

The molecular abundances that we used in the baseline model are summarized in Table II. Our choices were guided by previous work whenever possible and with trial runs of our model.

3.4.1. Arsine. Arsine was recently detected in both Saturn and Jupiter (Noll *et al.* 1989, Bézard *et al.* 1989) with mole fractions of 1.7×10^{-9} and 2.4×10^{-9}, respectively. We chose $qAsH_3 = 1 \times 10^{-9}$ for the baseline model because some of our preliminary fits indicated (erroneously as it turns out) that lower abundances might be more appropriate. As with PH_3 and

TABLE II
Molecular Abundances in the Baseline Model

Molecule	Mole fraction	
	Lower troposphere	Upper troposphere/ stratosphere
AsH_3	1 ppb	0.2 ppb
CH_3D	0.3 ppm	0.3 ppm
CO	2 ppb	2 ppb
GeH_4	0.4 ppb	0.08 ppb
NH_3	300 ppm at $P > 1.2$ bar	0 at $P < 160$ mbar
PH_3	7 ppm	1 ppm

GeH_4, we account for the expected photolytic destruction of AsH_3 in the stratosphere by reducing its mole fraction to 2×10^{-10} for $P < 400$ mbar and to zero at $P < 78$ mbar.

3.4.2. Deuterated membrane. Several determinations of CH_3D in Saturn were mentioned above (Courtin *et al.* 1984, Owen *et al.* 1986). An early estimate of the CH_3D abundance at 5 μm was made by Fink and Larson (1978), who obtained $CH_3D/CH_4 = 9 \times 10^{-5}$, leading to $CH_3D/H_2 = 4 \times 10^{-7}$ if we use the CH_4 abundance determination of Courtin *et al.* More recently, Bézard *et al.* (1987) reported agreement, on the basis of new 5-μm ground-based spectra, with the Courtin *et al.* CH_3D abundance from Voyager data. From these various results we adopted $q(CH_3D) = 3 \times 10^{-7}$ for our baseline model.

3.4.3. Carbon monoxide. Carbon monoxide was detected in Saturn by Noll *et al.* (1986) with a mole fraction of 2×10^{-9} if distributed throughout the troposphere or 3×10^{-7} if only in the stratosphere. We arbitrarily chose the tropospheric distribution for the baseline model since it was not possible to distinguish between these two possibilities with available data.

3.4.4. Germane. Germane was detected in Saturn by Noll *et al.* (1987). Noll *et al.* found $q(GeH_4) = 4 \times 10^{-10}$ while Bézard *et al.* (1987) reported a concentration similar to that in Jupiter. We adopted $q(GeH_4) = 4 \times 10^{-10}$ for our baseline model. Germane is likely to be photodissociated in the upper atmosphere so we reduced $q(GeH_4)$ by a factor of 5 to 8×10^{-11} for $P < 400$ mbar and to zero for $P < 78$ mbar.

3.4.5. Ammonia. The NH_3 abundance in our model is constrained to follow the saturation curve for $T < 155$°K, the condensation temperature, and it is assumed to be photolytically destroyed at $P < 190$ mbar where the abundance drops to zero. The NH_3 abundance at temperatures higher than the cloud condensation temperature is of greater importance. Only observations at 5 μm and at radio wavelengths probe below the NH_3 condensation level in Saturn. Fink *et al.* (1983) and Courtin *et al.* (1984) found evidence for subsolar NH_3 abundances [0.33 and 0.50 times the solar value $(N/H_2)_\odot = 2.2 \times 10^{-4}$, respectively (Anders and Grevesse 1989)]. On the other hand, radio observations (Marten *et al.* 1980, de Pater and Massie 1985) provided equivocal evidence for enhanced NH_3 in the deep atmosphere ($q(NH_3) = 5 \times 10^{-4}$ at $P > 3$ bars), but their estimate of $q(NH_3)$ was not well constrained for $P < 3$ bars. We chose an intermediate value, $q(NH_3) = 3 \times 10^{-4}$, for our baseline model.

3.4.6. Phosphine. The abundance of PH_3 is the most important compositional parameter in our model. Since almost 2000 PH_3 lines occur within the spectral passband of our Saturn observations, there are practically no isolated spectral features of PH_3. Instead, PH_3 acts almost like a continuum absorber, mimicking the effects of clouds. This behavior is evident in Fig. 14 which shows the effect of doubling $q(PH_3)$ from 5×10^{-6} to 1×10^{-5}.

Some earlier PH_3 abundance determinations in Saturn are summarized in Prinn *et al.* (1984) with all but one value in the range $(0.8–2.0) \times 10^{-6}$. Most of these values were retrieved from spectra at 3 and 10 μm that sample the atmosphere near the upper cloud ($P \sim 400–700$ mbar). The first PH_3 abundance determination at 5 μm (Larson *et al.* 1980) indicated a higher value than at 3 and 10 μm which the authors attributed to deeper atmospheric sounding at 5 μm and a constant tropospheric mixing ratio. Subsequent work at 5 μm (Noll 1987, Bézard *et al.* 1987) confirmed that the PH_3 mole fraction was much higher in deeper atmospheric levels (3×10^{-6} and 4×10^{-6}, respectively). We fixed $q(PH_3)$ in our baseline model at 1×10^{-6} for $P < 400$ mbar and at zero for $P < 78$ mbar to agree with the stratospheric vertical profile deduced by Tokunaga *et al.* (1980). At tropospheric levels we initially adopted PH_3 mole fractions of $(3–5) \times 10^{-6}$ following the recent work of Noll *et al.* (1987) and Bézard *et al.* (1987), but it was immediately evident that these values underestimated the strength of Saturnian features in the region 2000–2070 cm^{-1}. We therefore looked for independent observational evidence to establish a more realistic tropospheric distribution of PH_3 in the baseline model. After studying synthetic spectra of PH_3 we identified an isolated feature at 1972 cm^{-1} made up of low-J lines that could provide a potentially sensitive test of its tropospheric distribution. This spectral region is not included in our observations of Saturn, but it was covered recently by Noll and Geballe (unpublished data) at similar resolution and sensitivity. From preliminary fits to their data we retrieved a surprisingly large tropospheric mole fraction of PH_3: at least 7×10^{-6} and possibly more. When this value was used in our baseline model the fit to the region

2000–2070 cm^{-1} of our spectrum improved, although the fit from 2130 to 2160 cm^{-1} worsened slightly. Based on this improvement we chose $q PH_3 = 7 \times 10^{-6}$ for the baseline model.

4. DETERMINATION OF MOLECULAR ABUNDANCES

Since the determination of molecular abundances is the primary goal of this paper, careful selection of spectral features in the context of the observed planetary spectrum is crucial to the analysis of each atmospheric constituent. The complexity of Saturn's 5-μm spectrum means that very often the most diagnostic features of a molecule's spectrum will coincide with lines of other species, usually PH_3. The density of lines may be so high that a trace constituent may only *shift* the local continuum level rather than change the *shape* of a spectral feature. Unfortunately, the continuum spectrum is influenced by many factors, including the abundances of all other gaseous constituents and by the assumed cloud parameters. The most reliable abundance determinations depend on finding lines in relatively uncluttered regions of the observed spectrum that produce recognizable changes in spectral lineshapes. Features of AsH_3, CH_3D, CO, and NH_3 satisfy this criterion. Abundance estimates are less precise if candidate lines are so weak or densely spaced that changes in abundance produce only shifts in the local continuum level. Absorption by GeH_4 and PH_3 is in this category. We discuss each molecule individually in the following sections.

4.1. Arsine

Arsine is the most recently detected molecule in Saturn's atmosphere so basic questions concerning its abundance and distribution are still being addressed. In Fig. 6 we compare a spectrum of AsH_3 with three synthetic spectra of Saturn using $q AsH_3 = 0, 2 \times 10^{-9}$, and 4×10^{-9} in the baseline model. Many spectral features of AsH_3 are readily detectable in the sense that changes in $q AsH_3$ from 0 to a few $\times 10^{-9}$ produce differences in the baseline model that would be larger than the noise level in the observations. A list of potentially detectable AsH_3 features is given in Table III. Closer inspection of Fig. 6 shows that several locations between 2070 and 2100 cm^{-1} are extremely sensitive to the AsH_3 abundance. This is because low-J lines of the ν_1 and ν_3 P branches of AsH_3 occur here and because several of these lines coincide with microwindows in Saturn's thermal emission spectrum, thus enhancing their detectivity. The importance of these fortuitous coincidences is illustrated by the AsH_3 absorptions near 2073 cm^{-1}. The large differences in the model calculations are caused by relatively weak ν_3 $P7$ lines while the intrinsically stronger ν_1 $P7$ lines are not even detectable because they coincide with strong PH_3 lines near 2076 cm^{-1}. In contrast to this situation in the P branch, the ν_3 Q branch is a very poor indicator of abundance. The difference between no AsH_3 and some AsH_3 is readily observed, but the difference between $q AsH_3 = 2 \times 10^{-9}$ and 4×10^{-9} is only marginally detectable in the synthetic spectra and would probably be obscured by noise in observations.

We computed synthetic spectra in the interval 2060–2100 cm^{-1} with $q AsH_3$ ranging from 1×10^{-9} to 5×10^{-9}; three examples are included in Fig. 7. The residuals were minimized for $q AsH_3$ between 3×10^{-9} and 4×10^{-9}. Before adopting this range as the best fit to $q AsH_3$ we investigated the effect of the uncertain value of $q PH_3$ on the determination of $q AsH_3$. We computed spectra with $q PH_3 = 1 \times 10^{-5}$, close to the maximum abundance consistent with the overall fit of our model to the spectrum. With this PH_3 abundance residuals are minimized for $q AsH_3$ somewhat less than 2×10^{-9}. This sensitivity is mainly the result of changes in the continuum level in microwindows where AsH_3 absorptions are strongest. Finally, we used line-to-continuum depths of isolated AsH_3 features to determine $q AsH_3$. The AsH_3 lines most useful for this approach are at 2073.7 and 2082.6 cm^{-1} (see Fig. 7). From the apparent strengths of these distinctive spectral lines, we found that $q AsH_3 \sim 3 \times 10^{-9}$. This is consistent with $q PH_3$ being somewhat greater than the nominal value, but less than the maximum.

It is difficult to estimate the uncertainties that we should attach to the above estimates of $q AsH_3$. The narrow, isolated lines in the interval 2060–2100 cm^{-1} are sensitive enough to allow high precision, but upon consideration of all uncertainties we adopt $(3 \pm 1) \times 10^{-9}$ as our best fit value of $q AsH_3$. Our measurement is consistent with values from Noll *et al.* (1989, $1.8^{+1.8}_{-0.9} \times 10^{-9}$) and Bézard *et al.* (1989, $2.4^{+1.4}_{-1.2} \times 10^{-9}$) and it should be more reliable because of the somewhat smaller errors and the use of more diagnostic AsH_3 spectral features.

4.2. Deuterated Methane

The ν_2 fundamental band of CH_3D is centered at 2200 cm^{-1}, near the short-wavelength edge of Saturn's 5-μm window, so only the P-branch manifolds (2100–2200 cm^{-1}) are accessible in remote observations. Since CH_3D is not photochemically destroyed in the lower atmosphere nor does it condense at the tropopause in Saturn, $q CH_3D$ remains constant throughout the pressure range sampled in the observations. Consequently, the absorbing column encountered by reflected solar radiation is not negligible and the CH_3D manifolds are prominent even in regions of the spectrum dominated by solar reflected radiation. In Fig. 8 we compare three synthetic spectra of Saturn using

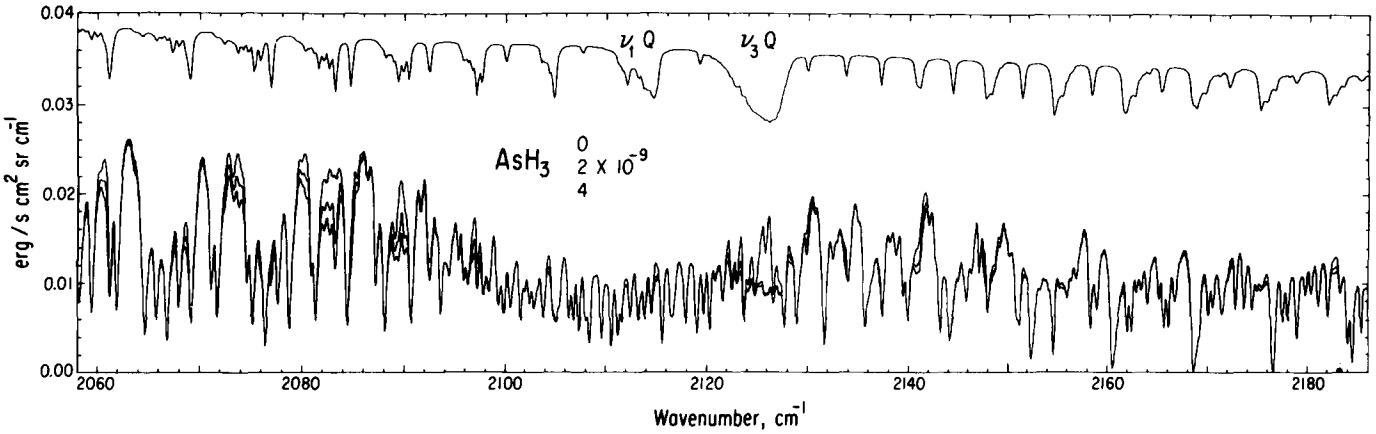

FIG. 6. Upper spectrum: Comparison spectrum of AsH_3. Lower composite: Calculations of Saturn's 5-μm spectrum for different AsH_3 mole fractions. The ν_3 Q branch provided the first evidence for AsH_3 in Saturn. The strengths of other AsH_3 features vary widely in Saturn, depending upon the net opacity of other atmospheric constituents. The ν_1 Q branch is marginally detectable at best while weak AsH_3 lines near 2080 and 2083 cm^{-1} generate prominent features in Saturn's spectrum due to their fortuitious coincidence with thermal microwindows.

qCH_3D = 0, 1.5 × 10^{-7}, and 6.0 × 10^{-7} with a spectrum of CH_3D alone. The maximum sensitivity to qCH_3D occurs for the $P7$ and $P8$ manifolds near 2144 and 2135 cm^{-1}, respectively. In Fig. 9 we compare sections of the observed spectrum that contain P-branch manifolds from $P9$ through $P4$ with model calculations for qCH_3D = 1.5 × 10^{-7}, 3.0 × 10^{-7}, and 6.0 × 10^{-7}. We also computed spectra with qCH_3D = 2.0 × 10^{-7} and 4.0 × 10^{-7} that are not shown. The best fit (from computed residuals as well as subjective criteria) is obtained with qCH_3D = (3.3 ± 1.5) × 10^{-7} which we use to calculate $(D/H)_{Saturn}$ in Section 6.1.

TABLE III
AsH_3 Spectral Features

Line position (cm^{-1})	Assignment	Detected?	New?
2060	ν_1 $P7$, ν_3 $P9$	Yes	Yes
2068	ν_3 $P8$, ν_1 $P6$	Yes?	
2074	ν_3 $P7$	Yes	Yes
2080	ν_3 $P6$	Yes	Yes
2082–2083	ν_3 $P6$	Yes	Yes
2089–2090	ν_3 $P5$	Yes	Yes
2092	ν_1 $P3$	No	
2097–2098	ν_3 $P4$	Yes?	
2115	ν_1 Q	Yes?	
2122–2127	ν_3 Q	Yes!	
2129	ν_1 $R1$	No	
2140	ν_3 $R1$	Yes?	
2182	ν_3 $R7$	?	

4.3. Carbon Monoxide

We detected as many as 13 individual lines of CO in Saturn, 8 of these for the first time (see list in Table IV). This positional evidence should eliminate any doubts that may have persisted about the presence of CO in Saturn. With so many lines to fit to our atmospheric model, we obtain not only a much better CO abundance estimate but also a chance to search for abundance variations with altitude. Both of these tasks are important to chemical

TABLE IV
CO Spectral Features

Line position (cm^{-1})	Assignment	Detected?	New?
2086.3	$P14$	Yes	Yes
2094.9	$P12$	No	
2119.7	$P6$	Yes	
2123.7	$P5$	Yes	
2127.7	$P4$	Yes	Yes
2131.6	$P3$	No	
2135.5	$P2$	Yes?	
2139.4	$P1$	Yes	
2147.1	$R0$	Yes	Yes
2150.9	$R1$	?	
2158.3	$R3$	Yes	
2162.0	$R4$	Yes	Yes
2165.6	$R5$	Yes	Yes
2169.2	$R6$	?	
2172.8	$R7$	Yes	Yes
2179.8	$R9$	Yes	Yes
2183.2	$R10$	Yes	Yes

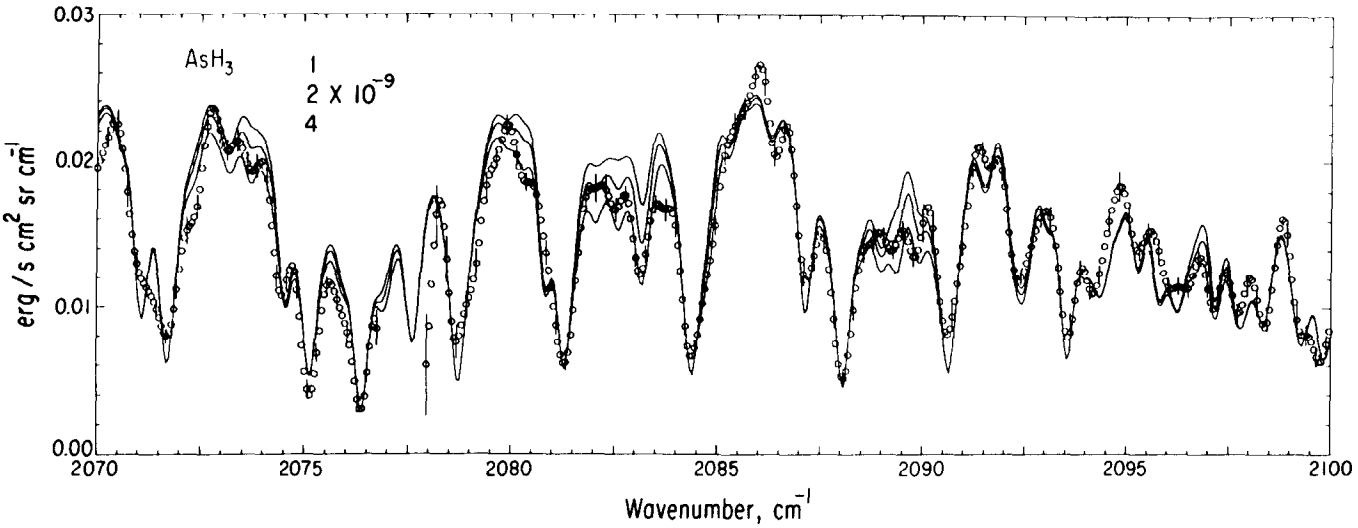

FIG. 7. Comparison of Saturn's observed spectrum (open symbols) with synthetic spectra calculated for three mole fractions of AsH_3 (solid lines). Vertical lines spaced once per resolution element indicate the rms noise in the observations. Although this spectral interval does not contain the prominent AsH_3 Q branches (see Fig. 6) it does provide the most sensitive measurement of $q$$AsH_3$ in Saturn using narrow lines such as those at 2073.7 and 2082.6 cm^{-1}.

models of Saturn since CO is the only O-bearing molecule that has yet been detected in its atmosphere. The only other candidate, H_2O, is potentially detectable in airborne observations, but if the situation for Jupiter is any guide, interpretation of its abundance and distribution has its own set of problems (e.g., Lunine and Hunten 1987, Gautier and Owen 1989).

Two sources have been proposed to account for the observed presence of CO in Saturn (Prinn and Barshay 1977, Prather *et al.* 1978). The two possibilities differ markedly in the variation of qCO with altitude. The first distribution assumes constant qCO at all altitudes. This is the vertical profile that one would expect if CO originated deep in the atmosphere and was carried to the upper troposphere by convective motion driven by Saturn's excess internal energy. We refer to this in the following discussion as distribution **T.** The second proposed source of CO is infalling material from Saturn's rings. Gaseous CO produced high in the atmosphere from photochemical reactions would build up above the stagnant layer (i.e.,

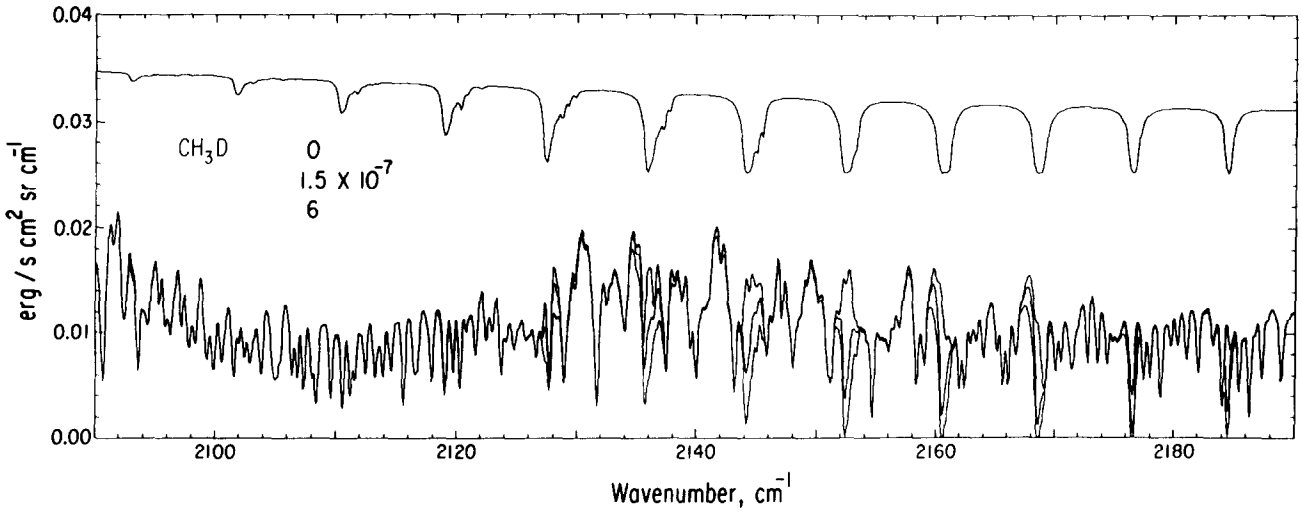

FIG. 8. Upper spectrum: Comparison spectrum of CH_3D. Lower composite: Calculations of Saturn's 5-μ spectrum for different CH_3D mole fractions. The CH_3D features with the strongest effect on Saturn's spectrum are the $P7$ and $P8$ manifolds at 2144 and 2135 cm^{-1}, respectively.

the tropopause near P = 50–200 mbar) that occurs at the top of the convective region close to the temperature minimum. Below the tropopause qCO would become that set by the internal source. We set the tropospheric abundance to $q\text{CO} = 1 \times 10^{-10}$, a value predicted in one chemical model of Saturn (Fegley and Prinn 1985). We designate this model as distribution **S.** The stratospheric distribution (distribution **S**) and the constant profile (distribution **T**) are compared in Fig. 10. We have not attempted

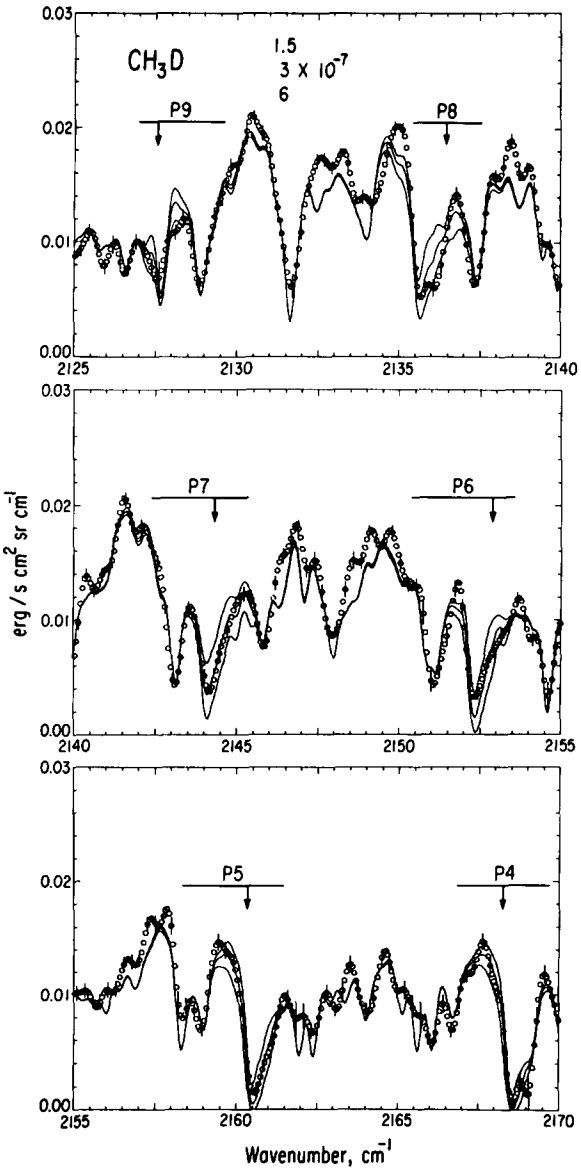

FIG. 9. Segments of Saturn's spectrum (open symbols) that include the strongest CH_3D manifolds. Vertical lines spaced once per resolution element indicate the rms noise in the observations. Three synthetic spectra of Saturn with different values of $q\text{CH}_3\text{D}$ are included for comparison (solid lines). The residuals between model and observations indicate that $q\text{CH}_3\text{D} = 3.3 \times 10^{-7}$ provides the best fit.

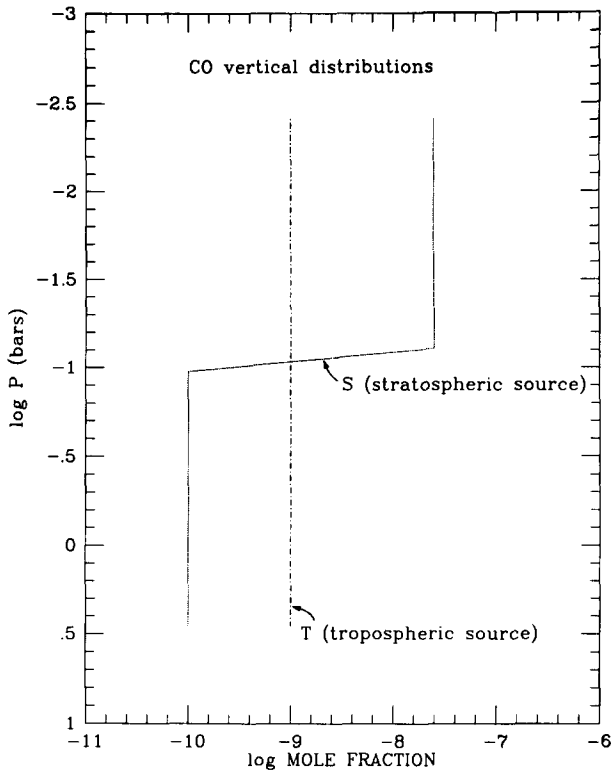

FIG. 10. The two vertical profiles used for CO. Profile T represents a tropospheric source of CO while profile S models an external source of material that would concentrate CO in the stratosphere.

to model the transition region between the stratospheric and tropospheric components of qCO in distribution **S.**

To investigate qCO and its variation with height we first fit the isolated $R0$ line for distributions **T** and **S.** We found that $q\text{CO} = 1 \times 10^{-9}$ worked well for profile **T** while $q\text{CO} = 2.5 \times 10^{-8}$ for $P < 80$ mbar gave an equally good fit for profile **S.** We then computed spectra covering the entire bandwidth in which we observed CO in Saturn (see Fig. 11). Distribution **T** with $q\text{CO} = 1 \times 10^{-9}$ provided an excellent fit to almost all of the 13 CO lines detected. The synthetic spectrum for distribution **S** is not shown in Fig. 11 because, with the exception of one line, it gave results that were indistinguishable from those for distribution **T.** This potentially important exception is discussed below.

An absorption feature at 2086.3 cm^{-1} in Saturn's observed spectrum (see Fig. 11) appears to be due to the $P14$ line of CO. Our synthetic spectra indicate that none of the other known absorbers in Saturn's 5-μm spectrum can account for this feature. Distribution **S** contributes negligible absorption at P14 because of the low stratospheric temperature, but distribution **T** with its higher tropospheric temperatures generates an observable line at the position of $P14$. The presence of this high-J feature

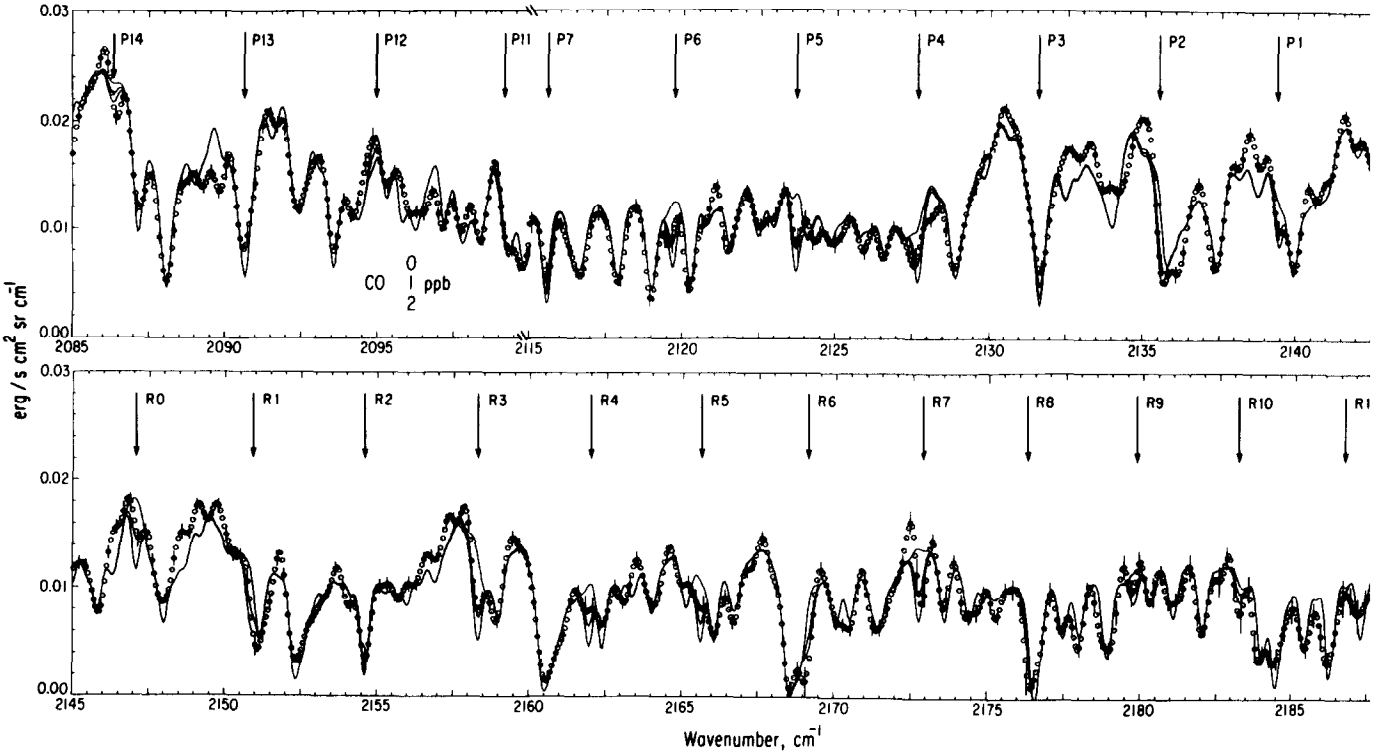

FIG. 11. Comparison of Saturn's observed spectrum (open symbols) with synthetic spectra calculated with different values of qCO (solid l for vertical distribution T (see Fig. 10). Vertical lines spaced once per resolution element indicate the rms noise in the observations. Twenty- lines of CO are coincident with these observations, 13 of which are detectable and 8 of which are observed here for the first time. The calcu spectra are clearly sensitive to the total column abundance of CO. Spectra calculated with the stratospheric distribution of CO are negli different. The one exception is the $P14$ line of CO at 2086.3 cm^{-1} that is coincident with a prominent, otherwise unassigned feature in Sat spectrum. This line is very weak in distribution S, but becomes stronger with distribution T.

favors a high rotational temperature for CO (perhaps even higher than we allowed in our model) and, consequently, for distribution **T** with abundant CO at warm temperatures below the tropopause. From the generally good fit of distribution **T** to other CO lines, particularly $R0$, we conclude that $q\mathrm{CO} = (1.0 \pm 0.3) \times 10^{-9}$, constant at all altitudes. We must emphasize, however, that this interpretation is based upon a single spectral feature, the $P14$ line, so improved observations are needed to confirm it. In the discussion in Section 6.2 we consider the implications of an internal origin of CO in Saturn; the implications of an external source have been discussed elsewhere (Noll *et al.* 1986).

4.4. Germane

Germanium has five naturally occurring isotopes, three of which have fairly high abundances. In addition, the measured pressure broadening coefficient is unusually high (Varanasi and Chudamani 1987). As a consequence, GeH_4 spectral features formed in planetary atmospheres are broad (~1.5 cm^{-1} wide) and shallow compared to isolated spectral lines. Coupled with its low abundance, a poor situation therefore exists for identifying and ana ing the abundance of GeH_4 in Saturn's atmosphere.

Seven spectral features of GeH_4 are potentially det able in our spectrum of Saturn (see Fig. 12). The $P4$, and $R6$ features provide a better match to Satu spectrum when $q\mathrm{GeH_4} = 4 \times 10^{-10}$ is included in model. The fit at $P3$ gets worse, however, while the f $R3$ and $R4$ is poor for reasons that apparently are unrel to the GeH_4 abundnce. Evidence for the wide Q bra consists of deviations between the model and obse tions at the local peaks in flux at 2109, 2110, and 2112 c (see Fig. 12). The match is clearly better when qGeH 4×10^{-10} is included in the model. Other deviation the region of the Q branch of GeH_4 are unexplai including a very prominent absorption in Saturn at 21 cm^{-1}. Absorption by PH_3 influences the neighborhc of each GeH_4 feature in Fig. 12 and AsH_3 absorptio important at the GeH_4 $P4$ line. Given all of these compl tions we conclude that available evidence favors the p ence of GeH_4 in Saturn, with abundance similar to assumed in the baseline model, but $q\mathrm{GeH_4} = 0$ canno excluded. Much higher abundances of GeH_4 than in

baseline model would cause unacceptably large absorption, particularly at the GeH_4 $P3$ line. We therefore adopt $q GeH_4 = (4 \pm 4) \times 10^{-10}$ as a conservative estimate of the abundance of GeH_4 in Saturn.

Upon comparison with the earlier work of Bézard *et al.* (1987) and Noll *et al.* (1988a) it should be noted that neither group included AsH_3 in their models since it had not yet been detected. Also, Noll *et al.* used an earlier compilation of PH_3 data that differs from the latest results of Tarrago *et al.* (1987). It is therefore possible that their analyses may have underestimated uncertainties due to spectral confusion caused by other absorbers. Our model is fit over a much broader spectral bandwidth than was possible in either of these two previous studies. This gives a better perspective on the GeH_4 abundance because the influence of other atmospheric constituents can be more critically assessed.

4.5. *Ammonia*

Ammonia does not have its strongest 5-μm spectral features in the interval covered by our observations. Many of the NH_3 lines that do occur here are coincident with pervasive PH_3 absorptions, as can be seen by comparing Figs. 13 and 14. A few NH_3 lines that produce potentially detectable modifications to the shape of Saturn's spectrum are identified in Fig. 13. Unfortunately, we have not been able to retrieve a consistent NH_3 abundance from these lines. Several features (e.g., 2014.0, 2025.0, 2032.1, 2040.3, and 2073.2 cm^{-1}) indicate that $q NH_3$ is close to the baseline value (3×10^{-4}) while others (e.g., 2010.1, 2011.8, and 2050.4 cm^{-1}) imply that $q NH_3$ is lower. This ambiguity is perplexing. One possible explanation suggested by radio studies (de Pater and Massie 1985) is that $q NH_3$ is not constant in the upper troposphere between the NH_3 cloud base and the NH_4SH cloud top where our spectral lines probe at 5 μm. However, detailed investigation of altitude-dependent NH_3 distributions are premature because of uncertainties introduced by PH_3 absorptions in this region of the spectrum. We therefore do not believe that a definitive NH_3 abundance determination is possible with these data. At best, we rule out abundances greater than the baseline value. We conclude that $q NH_3 \leq 3 \times 10^{-4}$ in the zone above Saturn's NH_4SH cloud and below the NH_3 saturation level. A more sensitive test of the NH_3 abundance may be possible using NH_3 lines at longer wavelengths in Saturn's 5-μm window.

4.6. *Phosphine*

As shown in Figs. 3 and 14, the entire region of Saturn's spectrum that we observed is strongly affected by PH_3. Considering the quality of fit evident in figures throughout this paper (e.g., Fig. 2) we note that the abundance chosen

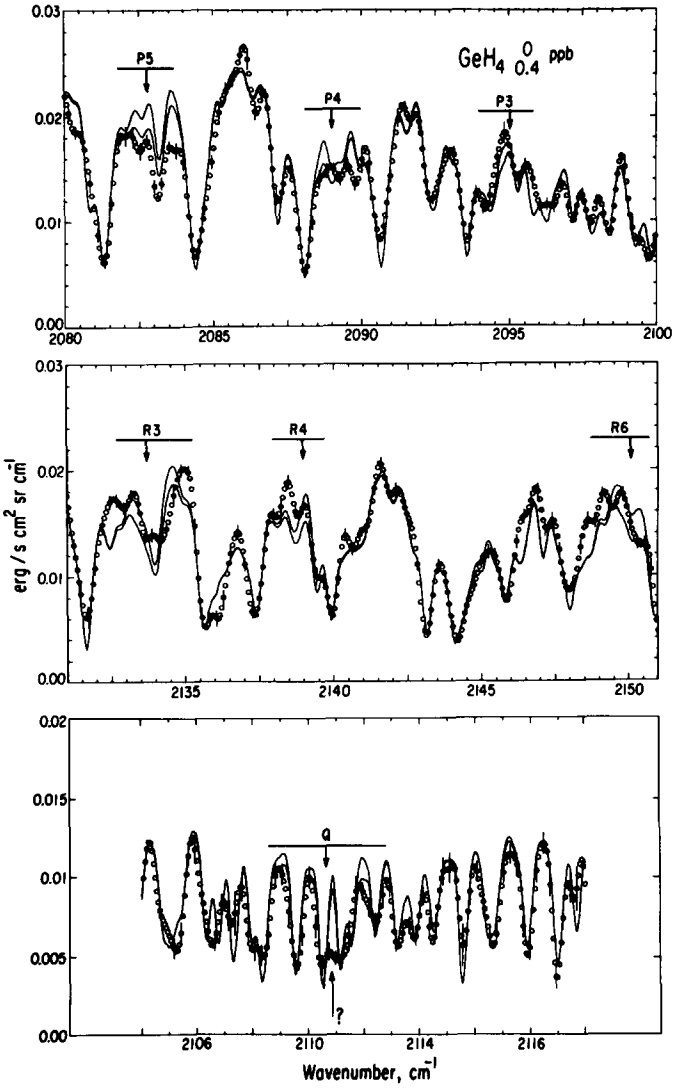

FIG. 12. Segments of Saturn's spectrum (open symbols) coincident with lines in the P, Q, and R branches of GeH_4. Vertical lines spaced once per resolution element indicate the rms noise in the observations. The solid curves are synthetic spectra calculated for two values of $q GeH_4$. The line-by-line evidence for GeH_4 is marginal due to intrinsically weak line strengths and unexplained deviations of the model from the observations near many of the GeH_4 lines.

for the baseline model, $q PH_3 = 7 \times 10^{-6}$, itself provides an excellent fit to the observations. We encountered several problems in attempting to refine this value, however. For example, the baseline model overestimates the intensity of many of the local intensity peaks from 2000 to 2060 cm^{-1} (see residuals in Fig. 15). In Section 3.4.6 we indicated that this part of the spectrum is strongly sensitive to the PH_3 abundance, but examination of Fig. 15 shows that there are no isolated PH_3 features that could be used to distinguish the effects of PH_3 from other continuum influences (i.e., clouds). From 2060 to 2130 cm^{-1} the

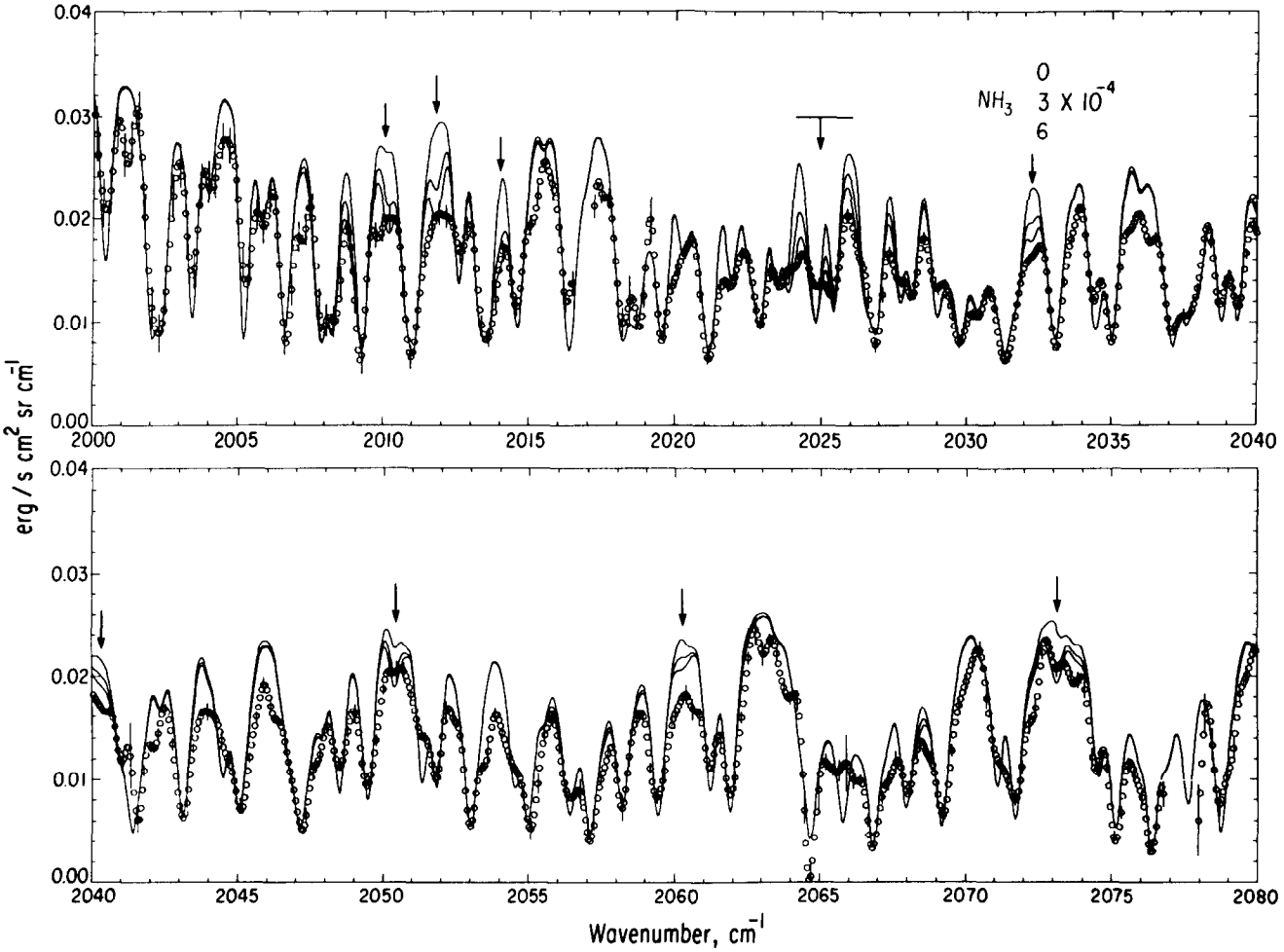

FIG. 13. Comparison of Saturn's observed spectrum (open symbols) with synthetic spectra calculated for three mole fractions of NH_3 (solid lines). Vertical lines spaced once per resolution element indicate the rms noise in the observations. The minimized residuals indicate large values of $q$$NH_3$, but critical examination of the depth of isolated NH_3 lines suggests that $q$$NH_3 \leq 3 \times 10^{-4}$. The mismatch between the observations and the model at many local peaks may be due to problems with PH_3 or to an unidentified absorber.

model does a much better job of matching peaks and valleys in the data (although the interval from 2100 to 2130 cm^{-1} is dominated by reflected sunlight), while from 2130 to 2160 cm^{-1} the model *underestimates* the height of local transmission peaks. These peaks represent at least 50% thermal radiation and therefore are sensitive to $q$$PH_3$ below the upper cloud. Our estimate of $q$$PH_3$ is a compromise based on fits to these several regions. A higher abundance improves the fit at lower frequencies while a lower abundance better accommodates the thermal microwindows from 2130 to 2160 cm^{-1} (see Fig. 5).

One reason that a completely satisfactory fit cannot be obtained with a single PH_3 abundance may be the abrupt change in our assumed vertical distribution profile from the lower tropospheric abundance $q$$PH_3 = 7 \times 10^{-6}$ to the upper tropospheric abundance $q$$PH_3 = 1 \times 10^{-6}$ at the position of the upper cloud. A more realistic treatment of the vertical profile of PH_3 could resolve these difficulties, but this task is beyond the scope of this paper. Despite this limitation, however, we confidently conclude that $q$$PH_3 = 7^{+3}_{-2} \times 10^{-6}$ in the troposphere of Saturn. This value is very high compared both to that in Jupiter (see Table VII) and to the solar abundance of P [$(P/H)_\odot = 3.7 \times 10^{-7}$ (Anders and Grevesse 1989)]. Even the lowest value of $q$$PH_3$ within the errors is eight times $(P/H)_\odot$, a result that may be an important constraint to models of planet formation (see Section 6.3).

5. THE "BEST-FIT" MODEL

With the exception of CO and AsH_3, only minor differences exist between the baseline model in Fig. 2 and the "best-fit" model that we present in Fig. 15. One of the most important accomplishments represented in this com-

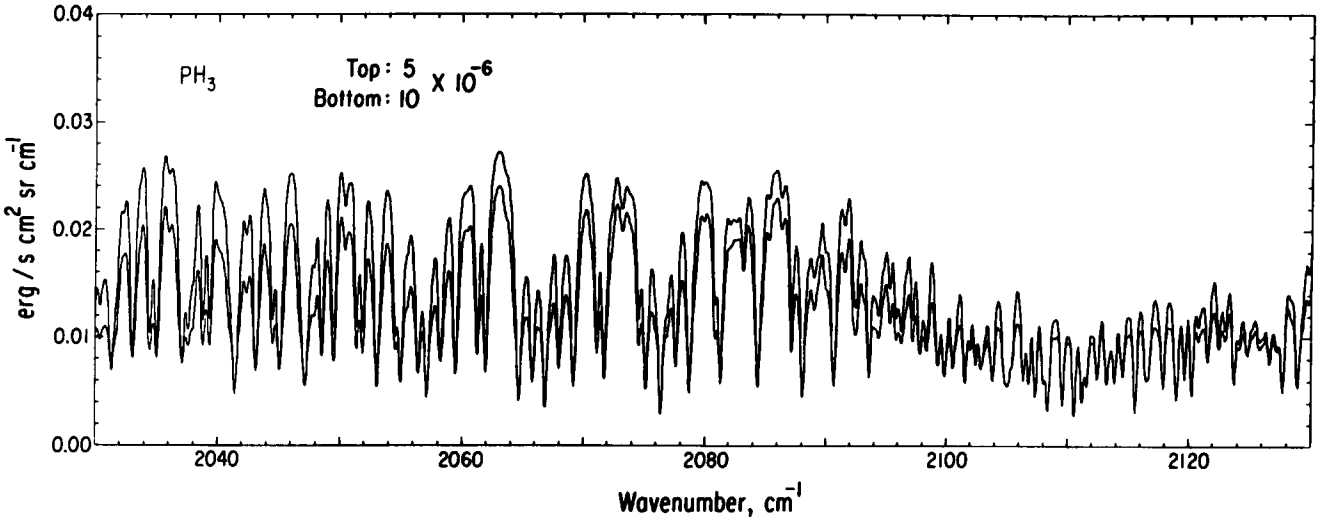

FIG. 14. The sensitivity of the atmospheric model to a factor of 2 change in $q\mathrm{PH_3}$ is illustrated. The abundances of all other constituents are held at their baseline values. The effect on Saturn's spectrum of increasing $q\mathrm{PH_3}$ is to lower the continuum rather than to produce deeper $\mathrm{PH_3}$ lines.

parison is the success in fitting $\mathrm{PH_3}$ across the transition region from reflected solar flux to thermal emission. The fit also confirms the surprisingly high abundance of $\mathrm{PH_3}$ that was suggested in earlier work and it demonstrates the major role of this gas in forming Saturn's 5-μm spectrum. In Fig. 15 we superimposed the best-fit model and the observed spectrum. To emphasize discrepancies, we also plot their difference smoothed by a moving boxcar of width equal to the instrumental resolution. Some of the major discrepancies are discussed in Section 5.1. The thousands of absorption features that contribute to this spectrum make it impossible to display all information clearly in a single figure. We therefore enlarged two sections of this spectrum (see panels *b* and *c* in Fig. 15) to reveal the detailed fit between the model (solid line) and the observations (dashed line). Most of the preceding figures contain similarly expanded displays of other regions of Saturn's spectrum.

The column abundances and mole fractions used to generate the best-fit spectrum are summarized in Table V. The reader should remember that these retrieved parameters are dependent on model assumptions, particularly the location of the lower cloud. For molecules with weak absorptions in the thermal portion of the spectrum, such as CO and $\mathrm{AsH_3}$, the column abundance will not change if the cloud is moved deeper in the atmosphere, but the inferred mole fraction will change in inverse proportion to the increase in pressure. On the other hand, molecules primarily in the reflected portion of the spectrum are insensitive to the lower cloud and depend instead on the location of the upper cloud, its reflectivity, and the accuracy of the simple reflecting layer approximation. Many $\mathrm{PH_3}$ lines and the *Q* branch of $\mathrm{AsH_3}$ are in this category, whereas $\mathrm{CH_3D}$ is an intermediate case with sensitivity to the properties of both cloud layers.

TABLE V
Best-Fit Molecular Abundances

Molecule	Column abundance (cm-amagat)	Mole fraction
$\mathrm{AsH_3}$	0.088	3 ± 1 ppb
$\mathrm{CH_3D}$	11.0	0.33 ± 0.15 ppm
CO	0.034	1.0 ± 0.3 ppb
$\mathrm{GeH_4}$	0.012	0.4 ± 0.4 ppb
$\mathrm{NH_3}$	5922	≤300 ppm
$\mathrm{PH_3}$	207	7^{+3}_{-2} ppm

5.1. *Unidentified Spectral Features*

The difference spectrum in Fig. 15 is useful for identifying spectral features that are not reproduced by the model. The height of the stippled region equals four times the mean error in the observations. Differences that exceed this level could arise from several situations, including species not included in the model, missing lines of known species, erroneous line parameters, or failure of the model to represent physical conditions in Saturn's atmosphere. Our detailed inspection of many of these features suggests that they are due primarily to very small differences in line position or linewidth. This situation is particularly prevalent in the interval 2000–2050 $\mathrm{cm^{-1}}$, but this explanation appears inadequate for all features in the difference spectrum. Table VI contains a list of features associated with large residuals that we consider most

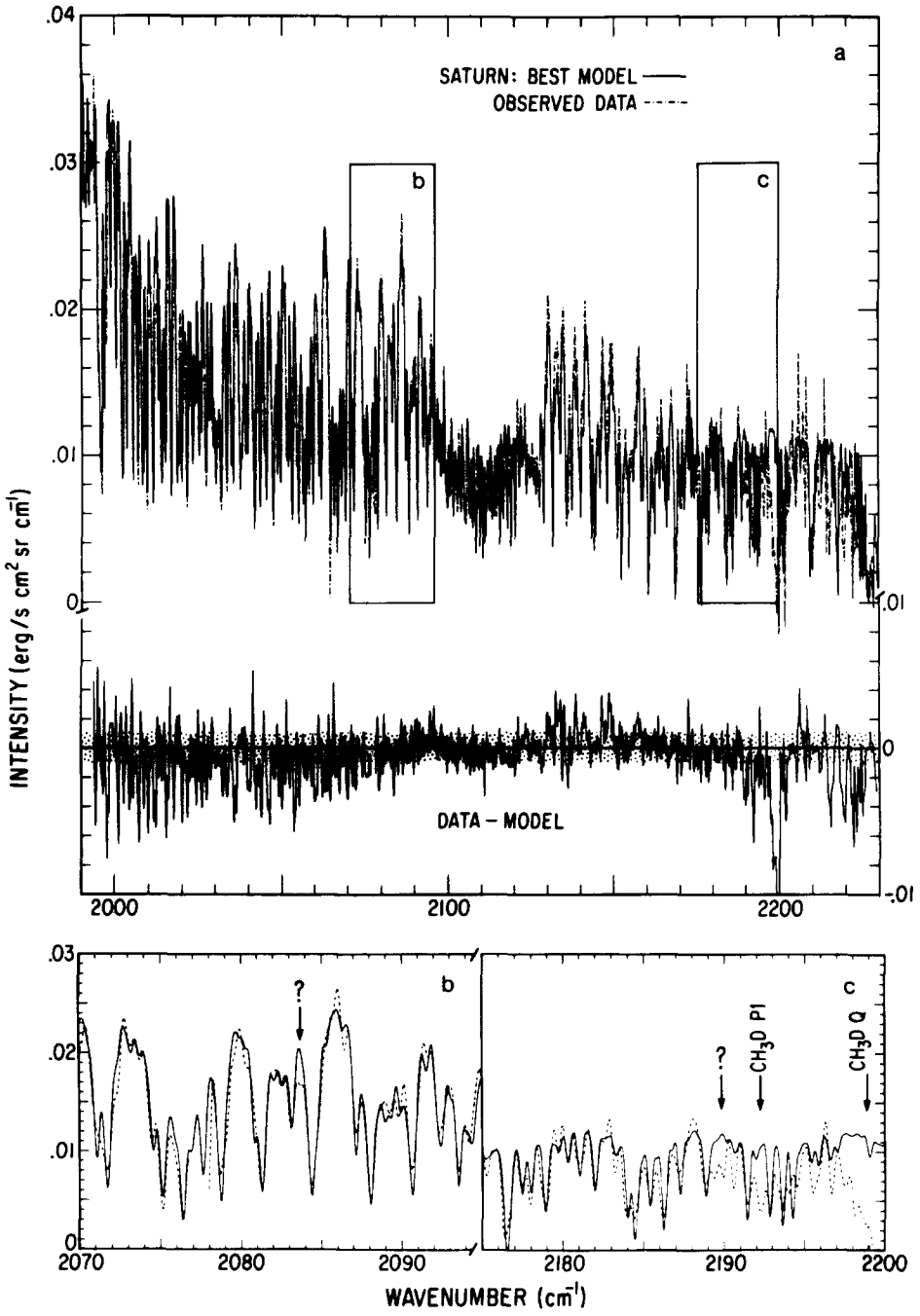

FIG. 15. (a) The observed spectrum of Saturn and the best-fit synthetic spectrum are superimposed to demonstrate their overall agreement. The residuals are plotted to reveal discrepancies that could be associated with unidentified constituents or deficiencies in the model. (b, c) Details of the fit between the model (solid line) and observations (dashed line). Several discrepancies are noted that could be unidentified species in Saturn; other deviations are due to missing lines in the molecular data or to slight mismatches in line positions.

likely to be caused by missing spectral lines. Most entries indicate the positions at which Saturn's spectrum has additional absorption that is not accounted for by the model. A smaller number of features occur where the model significantly overestimates the amount of absorption present in Saturn's spectrum. Some of these deviations could be due to large uncertainties in the ratio spectrum near strong telluric lines. The P1 line and Q branch of CH_3D, for which molecular line parameters are not available (see Section 3.4.2), account for the mismatches at 2192.2 and 2197–2200 cm^{-1}, respectively. We include possible assignments to some entries in Table VI based

TABLE VI
Unidentified Spectral Features

Position (cm^{-1})	Type	Possible assignment
1998.2	Abs	?
2001.1	Abs	?
2007.2	Abs	?
2009.8	Abs	NH_3
2015.2	Abs	?
2019.9	Abs	?
2021.6	Abs	?
2035.6	Abs	?
2041.3	Em	$\oplus$
2051.3	Em	?
2063.1	Abs	?
2065.8	Em	$\oplus$
2083.6	Abs	AsH_3, GeH_4
2110.9	Abs	GeH_4
2132.5	Em	PH_3
2189.6	Abs	?
2190.5	Abs	?
2192.2	Abs	CH_3D *P*1
2194.3	Em	$\oplus$
2195.6	Abs	$\oplus$
2197–2200	Abs	CH_3D *Q*

on coincidences with lines of known constituents. One particularly intriguing feature is the relatively broad absorption at 2189.6 cm^{-1}. It is several resolution elements wide so it is most likely formed by more than one spectral line. We considered that it might be a signature of the *Q* branch of SiH_4, but the position is not compatible with high-resolution laboratory comparison spectra of SiH_4 (see Section 5.2). For most of the entries in Table VI, however, we have no clues whatsoever to their identify. Their presence emphasizes that there is still information to be gleaned from additional studies of Saturn's atmosphere at 5 μm.

5.2. Upper Limit to SiH_4

Strict upper limits to the abundance of SiH_4 in Jupiter and Saturn have already been made based upon the absence of its ν_3 *Q* branch at 2188.6 cm^{-1} [$<2.5 \times 10^{-9}$ (Treffers *et al.* 1978); $<1.2 \times 10^{-9}$ (Larson *et al.* 1980)]. In principle we could set a more stringent upper limit to $q$$SiH_4$ in Saturn because of the higher resolution of our data and the ability of our model to represent all known absorbers in the spectral region containing the *Q* branch of SiH_4. Unfortunately, laboratory analyses of SiH_4 are not available for use in spectrum synthesis applications. Larson (unpublished data) has room temperature laboratory comparison spectra of SiH_4 at several abundances, but in all cases the *Q* branch is saturated and therefore not very useful for extrapolation to the very low abundances appropriate to Saturn's atmosphere. To get a first-order estimate of the sensitivity of our model to SiH_4, we simulated its presence using molecular parameters for the *Q* branch of GeH_4 shifted to the higher frequency position of the SiH_4 *Q* branch. This approximation may not be too bad since both molecules are spherically symmetric tetrahedra, although the GeH_4 *Q* branch is a combination of the ν_3 and ν_1 modes while the SiH_4 *Q* branch consists of ν_3 only. With this approximation we found that the frequencies most sensitive to the presence of SiH_4 are in a thermal microwindow from 2187.5 to 2188.5 cm^{-1}. If the band strength of the *Q* branch of SiH_4 is identical to that for GeH_4, calculations indicate that we could detect SiH_4 at the level of $q$$SiH_4 = 2 \times 10^{-10}$. Calling f the ratio of the GeH_4 and SiH_4 band strengths, we express our upper limit as $q$$SiH_4 \leq 2 \times 10^{-10} f$. If f is close to unity our upper limit to SiH_4 in Saturn is six times lower than the earlier estimate of Larson *et al.* (1980). A useful application of the SiH_4 upper limit is discussed in Section 6.2 below.

6. DISCUSSION

Three principal results of this work merit discussion. First, our measured abundance of CH_3D is of interest because of the cosmogonic significance of D/H ratios in the giant planets. Second, our measured abundance of CO can be related to the elemental abundance of O in Saturn's atmosphere. Finally our measured abundances of AsH_3 and PH_3 may be important observational constraints to models of the formation of the outer planets.

6.1. The D/H ratio in Saturn

The abundance of deuterium in the outer solar system has been reviewed many times (e.g., Gautier and Owen 1989 and references therein). The special attention devoted to this topic is due to the diagnostic value of the D/H isotopic ratio to solar nebula models. On the one hand, the atmospheres of Jupiter and Saturn may have preserved the D/H ratio in the primordial solar nebula. In principle, evolution of D/H in the galaxy over the last 4.5 billion years can be measured and the baryon density of the universe determined, both problems of considerable cosmological interest. Measurements of D/H in solar system bodies are also important in tracing the origin of volatiles in planetary atmospheres because deuterium fractionation occurred in ices in the presolar nebula.

The current best estimate for D/H in Saturn is $(D/H)_{Saturn} = (1.7^{+1.9}_{-1.0}) \times 10^{-5}$ (Gautier and Owen 1989). To calculate $(D/H)_{Saturn}$ using our measured CH_3D abundance, we must adopt a CH_4 abundance from another spectral analysis. Gautier and Owen chose $CH_4/H_2 = (4 \pm 2) \times 10^{-3}$ from the work of Buriez and de Bergh (1981). Using a fractionation factor of 1.229 for Saturn (Fegley and Prinn 1988b) we obtain $(D/H)_{Saturn} = \frac{1}{4} \times (1/1.229) \times (3.3 \times 10^{-7})/(4 \times 10^{-3}) = 1.7 \times 10^{-5}$. Upon propagating

the errors in the molecular abundance determinations, we conclude that $(D/H)_{Saturn} = (1.7 \pm 1.1) \times 10^{-5}$. This is almost identical to the ratio derived by Gautier and Owen, but it is only partially independent of their analysis since we adopted the same value for the CH_4 abundance as they did. We reduced the uncertainty in the upper bound to $(D/H)_{Saturn}$ by ~60%. The D/H ratio adopted by Gautier and Owen for Jupiter is $(D/H)_{Jupiter} = (2.1 \pm 0.6) \times 10^{-5}$. The upper bounds to the D/H ratios in Saturn and Jupiter are now approximately the same, although it is still possible for $(D/H)_{Saturn}$ to be substantially lower than $(D/H)_{Jupiter}$. It is interesting to note that uncertainty in the CH_4 abundance contributes more than half of the error in $(D/H)_{Saturn}$. Additional progress will therefore depend as much on improved CH_4 determinations as on refined analyses of CH_3D.

6.2. *The Abundance of Oxygen in Saturn*

One intriguing aspect of studying CO in Saturn is that it leads to an indirect assessment of the abundance of O in its deep atmosphere. The arguments are involved and have many uncertainties. In addition, we remind the reader that the evidence for an internal source of CO is still weak. However, any observational link that places *possible* limits on Saturn's O abundance relative to Jupiter's is worth developing. We therefore proceed on the assumption, whether supported strongly by the specific results of this paper or not, that CO has an internal origin in Saturn. The CO present in the upper troposphere would then be due to rapid transport from hot levels of the atmosphere to the cooler troposphere on a time scale shorter than the chemical reactions that would otherwise convert it to CH_4. A theoretical description of this process was presented by Prinn and Barshay (1977) to explain the observed presence of CO in Jupiter. Fegley and Prinn (1985) used this same technique for Saturn to predict a tropospheric CO abundance of 1.3×10^{-10}, 7.7 times less than our measurement. Three parameters affect the amount of CO transported into the troposphere. One is the chemical reaction time, which is the same for Jupiter and Saturn. The second is the vertical transport time. If we assume that the simple mixing-length model adequately predicts the mean rate of vertical transport in the outer planets, then the eddy mixing coefficient which measures the vertical transport time is as well known in Jupiter as in Saturn. That leaves only the abundances of C and O in the deep atmosphere as variables. Fegley and Prinn fixed all elemental abundances at 2.5 times solar values in their Saturn model while Prinn and Barshay assumed solar abundances for all elements in Jupiter's deep atmosphere. In Table II in Gautier and Owen (1989), Saturn's measured C abundance is in the range $(2 - 6) \times (C/H)_\odot$ (the best being 5.5 times solar) while $(C/H)_{Jupiter} = (2.32 \pm 0.18) \times (C/H)_\odot$. Uncertainties in the chemical reaction and vertical transport times are large enough that they can accommodate the differences in elemental abundances between observations and the model and still reproduce the observed CO abundance. If we fix $(C/H)_{Saturn}$ at $5.5 \times (C/H)_\odot$, then Saturn's deep O abundance is the only remaining parameter that affects its tropospheric CO abundance. In summary, therefore, we assume (1) that CO is brought up from the hot interior by vertical mixing that quenches the CO–CH_4 reactions the same in Jupiter and Saturn, (2) that mixing rates are as well known in Saturn as in Jupiter, and (3) that the thermochemical model successfully predicts the observed amount of CO in Jupiter for $(C/H)_{Jupiter} = 2.32 \times (C/H)_\odot$ and an undetermined O abundance. Then we ask if $(C/H)_{Saturn} = 5.5 \times (C/H)_\odot$, what must $(O/H)_{Saturn}$ be relative to $(O/H)_{Jupiter}$ to match the observations?

Thermochemical models for Jupiter with solar C and O predict $q\mathrm{CO} = 1 \times 10^{-9}$ in the upper troposphere 1.3 times less than observed. The same model applied to Saturn, but with C and O abundances set at 2.5 times solar values, predicts that $q\mathrm{CO} = 1.3 \times 10^{-10}$, 7.7 times less than observed. The mean C abundance that we assumed in Saturn relative to Jupiter is negligibly different than the 2.5 times enhancement assumed in the models. Therefore, if the difference between the observed and predicted CO abundances in Saturn is to be made up by O (already 2.5 times more abundant in the Saturn model), its deep abundance would have to be increased still further by the factor 7.7/1.3 for a total enrichment of $(7.7/1.3) \times 2.5 \approx 15$ relative to Jupiter.

A second constraint on Saturn's O abundance is derived from our observed upper limit to SiH_4 in Section 5.2. This method places a speculative lower limit on the *absolute* O abundance in Saturn's atmosphere, whereas the argument based on CO gives only the *relative* O abundance in Saturn compared to Jupiter. Fegley and Prinn (1988a) argued from cosmic abundances that the ratio $O/(Mg + 2Si) \geq 1$ in Jupiter based on the observed upper limit to SiH_4. This relation is valid for $q\mathrm{SiH_4}$ as high as 10^{-6} and it is readily extended to Saturn because the arguments do not depend strongly on details of Jupiter's interior. We do not know the elemental abundances of Si and Mg in the envelope of Saturn so we cannot use Fegley and Prinn's inequality directly to estimate the abundance of O in Saturn. We speculate, however, that Mg and Si in Saturn's deep atmosphere are enriched to the same degree as As and P at tropospheric levels, namely, 5–10 times the solar abundance. For 5 times enrichment of Mg and Si the inequality implies that the elemental abundance of O in Saturn is greater than 0.6 times the solar value. How much greater could it be? If O in Saturn is enriched by the same amount as other elements that originated in the condensed portion of the presolar nebula, it could be as much as 10 times the

solar value. Such a large enrichment is compatible with models of Saturn's interior based on measured gravitational moments (Hubbard, private communication), and cannot be rule out a priori because other elements such as P and As also show large enrichments in Saturn relative to Jupiter. We discuss this and other elemental abundances in the context of models of planetary formation in the next section.

6.3. *Enrichment of Heavy Elements in Saturn*

The observed spectra of Jupiter and Saturn at 5 μm are compared in Fig. 16. The Jovian spectrum was obtained at the Kuiper Airborne Observatory (Larson *et al.* 1977). The elemental abundances in their deep atmospheres inferred from these and other spectra are summarized in Table VII. All elements heavier than He appear to be enhanced in Saturn to a greater degree than in Jupiter. This trend, which holds (at least for C) for Uranus and Neptune as well, has been attributed to larger core-to-envelope mass ratios as one moves from Jupiter through the other outer planets. While this may in general be true, the models may be too simplistic to explain some of the differences that seem to exist between elements.

Several problems present themselves when one attempts to understand elemental abundances in the atmospheres of the outer planets. If one accepts the inhomogeneous accretion model for the formation of the outer planets (e.g., Pollack and Bodenheimer 1989) one needs to know the physical state (gas or solid) of each element

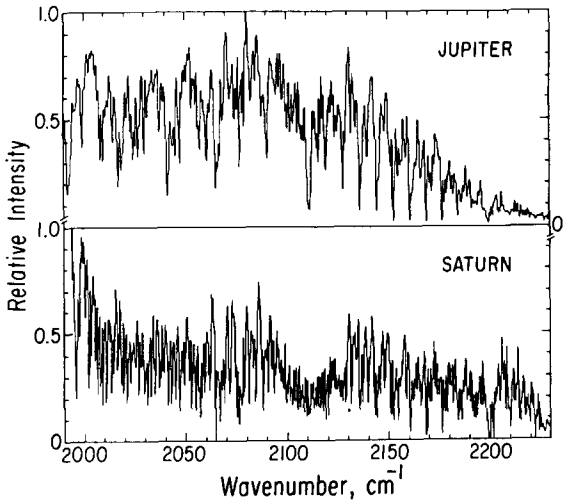

FIG. 16. Comparison of spectra of Jupiter and Saturn at 5 μm. Both spectra are formed by the same six molecules in Fig. 3, but their different appearance is due primarily to the much higher abundance of PH_3 in Saturn. The Q branch of GeH_4 that is so prominent in Jupiter at 2111 cm^{-1} is not evident in Saturn, while the evidence for AsH_3 in both planetary atmospheres depends upon careful modeling of all constituents.

TABLE VII
Abundances in Jupiter and Saturn

Molecule	Jupiter	Saturn
AsH_3	0.22 ± 0.11 ppb[a]	3 ± 1 ppb
CH_3D	0.20 ± 0.04 ppm[b]	0.33 ± 0.15 ppm
CO	1.3 ± 0.3 ppb[b,c]	1.0 ± 0.3 ppb[d]
GeH_4	$0.7^{+0.4}_{-0.2}$ ppb[b]	0.4 ± 0.4 ppb
NH_3	260 ± 40 ppm[b]	≤300 ppm
PH_3	0.7 ± 0.1 ppm[b]	7^{+3}_{-2} ppm

[a] Noll and Larson 1990.
[b] Bjoraker *et al.* 1986a.
[c] Noll *et al.* 1988b.
[d] Uniform vertical distribution assumed.

since the two phases are incorporated into the growing planets in very different ways. For example, much of the C in the presolar nebula may have been in the form of gaseous CO (Lewis and Prinn 1980, Simonelli *et al.* 1989), but there are many unanswered questions. One way to avoid such complications is to study elements that were present in the nebula only in the condensed phase when the planets were being formed. An elemental abundance observed in the atmosphere is then a function only of the overall heavy element abundance of the planet and the degree to which the solid component was mixed into the gaseous envelope. In the formalism of Simonelli *et al.* (1989) the enrichment equation [their Eq. (2)] $E_{g/H} = (1 - \alpha_g) + \alpha_g\beta_g\ (F_{HZ}/F_S)$ becomes $E_{g/H} = \beta_g\ (F_{HZ}/F_S)$ for the limiting case of an element g that is completely condensed ($\alpha_g = 1$). The remaining symbols are defined as follows. β_g is the fraction of element g that is mixed into the envelope, either by dissolution of late-accreting planetesimals (Pollack *et al.* 1986) or by vaporization of core material and later mixing during convection initiated by hydrodynamic collapse of the surrounding nebular gas (Owen, private communication). F_{HZ} is the mass ratio of high-Z material (proton number $Z > 2$) to low-Z gas in the present-day giant planets, and F_S is this ratio in the solar nebula prior to planet formation. To compare the results for As and P with those for C we will use the F_{HZ} and F_S values of Simonelli *et al.* If we set $\beta = 0.5$, one of the cases considered for C, then $E_{r/H} = 5.2$ for Jupiter and 13 for Saturn, where $E_{r/H}$ represents the enrichment of a rock-forming element ($\alpha = 1$) relative to the solar value. Both As and P are in this category. In addition, at least 50% of the O is in the solid phase.

The observed abundances of As and P in Jupiter and Saturn are in fact much different than predicted by this simple model. Saturn has ~10 times more As and P in its atmosphere than does Jupiter. The same pattern for O would also be consistent with the observed CO abundances. At least two explanations are possible. First, as

Pollack and Bodenheimer (1989) point out, the PH_3 abundance merely sets a lower limit to the atmospheric concentration of P. Phosphorous could also be bound in other molecules that have not yet been detected spectroscopically. The same argument applies to As. Thermochemical calculations (Fegley and Prinn 1985) indicate, however, that PH_3 and AsH_3 should be the dominant P- and As-bearing molecules in the upper troposphere when vertical transport is considered. A second possible explanation is that the assumed value of β (0.5) is incorrect. We easily calculate that $\beta = 0.05$–0.10 is required for Jupiter and $\beta = 0.25$–0.45 is necessary for Saturn to account for their observed As and P abundances. It is reasonable to expect that β, the fraction of incoming planetesimal material dissolved in the gaseous envelope, would be smaller for refractory materials than for ices or organic materials, but it is difficult to explain why this value should be lower for Jupiter which has a much more extensive envelope than does Saturn.

Both the measurements of elemental abundances in planetary atmospheres and models of planetary formation that attempt to explain observed compositions are in early stages of development. The unexpectedly high abundance determinations for As and P in Jupiter and Saturn provide an important observational test for the emerging models of giant planet formation.

7. CONCLUSIONS

The overall success of our atmospheric model in reproducing the spectrum of Saturn at 5 μm demonstrates significant progress in understanding the chemical composition and thermophysical description of its atmosphere. Principal uncertainties that remain include the pressure and optical depth of the lower cloud and their effects on mole fractions derived from observed column abundances. We estimate that uncertainties in our retrieved mole fractions are <50%. Most molecular absorbers have been identified since few spectral features are not reproduced by the model.

Two of the six molecules that we analyzed had mole fractions significantly different than in the baseline model. Arsine is present with a mole fraction higher than previously estimated, $q\mathrm{AsH_3} = (3 \pm 1) \times 10^{-9}$ below the upper cloud. Carbon monoxide is less abundant than reported previously, mainly because improved models represent the reflected component of the 5-μm spectrum more realistically. The mole fraction of CO is $(1.0 \pm 0.3) \times 10^{-9}$ if CO is uniformly concentrated at all altitudes and $(2.5 \pm 1.0) \times 10^{-8}$ if it is concentrated in the stratosphere instead. The presence of an absorption line near the expected location of the $P14$ line of CO hints at a tropospheric (warm) distribution. If so, we suggest that $(\mathrm{O/H})_{\mathrm{Saturn}}$ may be up to $15 \times (\mathrm{O/H})_{\mathrm{Jupiter}}$. The As/H and P/H ratios follow a similar pattern, in both cases ~10 times higher in Saturn. The observed enrichments of As and P do not agree with simple enrichment models. It appears that the mixing of heavy elements from the solids that helped form the planets into the atmosphere was more efficient in Saturn than in Jupiter. This agrees in general with interior models derived from gravitational moments that show Saturn has a greater concentration of heavy elements in its envelope than does Jupiter.

ACKNOWLEDGMENTS

We thank Bill Hubbard and Jonathan Lunine for helpful discussions. This work was supported by NASA Grant NAG 2-206.

REFERENCES

ANDERS, E., AND N. GREVESSE 1989. Abundances of the elements: Meteoritic and solar. *Geochim. Cosmochim. Acta* **53,** 197–214.

BÉZARD, B., P. DROSSART, E. LELLOUCH, J. P. MAILLARD, AND G. TARRAGO 1988. Evidence for arsine (AsH_3) in Saturn's atmosphere. *Bull. Amer. Astron. Soc.* **20,** 879.

BÉZARD, B., P. DROSSART, J. P. MAILLARD, G. TARRAGO, N. LACOME, G. POUSSIGUE, A. LEVY, AND G. GUELACHVILLI 1987. High resolution spectroscopy of Saturn at 5 μm. II. Cloud structure and gaseous composition. *Bull. Amer. Astron. Soc.* **19,** 849.

BÉZARD, B., P. DROSSART, E. LELLOUCH, G. TARRAGO, AND J. P. MAILLARD 1989. Detection of arsine in Saturn. *Astrophys. J.* **346,** 509–513.

BJORAKER, G. L., H. P. LARSON, AND V. G. KUNDE 1986a. The gas composition of Jupiter derived from 5-μm airborne spectroscopic observations. *Icarus* **66,** 579–609.

BJORAKER, G. L., H. P. LARSON, AND V. G. KUNDE 1986b. The abundance and distribution of water vapor in Jupiter's atmosphere. *Astrophys. J.* **311,** 1058–1072.

BURIEZ, J. C., AND C. DE BERGH 1981. A study of the atmosphere of Saturn based on methane line profiles near 1.1 μm. *Astron. Astrophys.* **94,** 382–390.

CHACKERIAN, C., AND G. GUELACHVILI 1983. Direct retrieval of line-shape parameters: Absolute line intensities for the ν_2 band of CH_3D. *J. Mol. Spectrosc.* **97,** 316–332.

CHEDIN, A., N. HUSSON, N. A. SCOTT, I. COHEN-HALLALEH, AND A. BERROIR 1986. *The "GEISA" Data Bank 1984 Version*, revised 1986. Laboratoire de Météorologie Dynamique du C.N.R.S. Internal Note LMD No. 127.

CHUDAMANI, S., AND P. VARANASI 1987. Measurements on 4.7 μm CH_3D lines broadened by H_2 and N_2 at temperatures relevant to planetary atmospheres. *J. Quant. Spectrosc. Radiat. Transfer* **38,** 179–181.

CONRATH, B. J., D. GAUTIER, R. A. HANEL, AND J. S. HORNSTEIN 1984. The helium abundance of Saturn from Voyager measurements. *Astrophys. J.* **282,** 807–815.

COURTIN, R., D. GAUTIER, A. MARTEN, AND B. BÉZARD 1984. The composition of Saturn's atmosphere at northern temperate latitudes from Voyager IRIS spectra: NH_3, PH_3, C_2H_2, C_2H_6, CH_3D, CH_4, and the Saturnian D/H isotopic ratio. *Astrophys. J.* **287,** 899–916.

DE PATER, I., AND S. T. MASSIE 1985. Models of the millimeter-centimeter spectra of the giant planets. *Icarus* **62,** 143–171.

DRAEGERT, D. A., AND D. WILLIAMS 1968. Collisional broadening of CO absorption lines by foreign gases. *J. Opt. Soc. Amer.* **58,** 1399–1403.

DROSSART, P., B. BÉZARD, J. P. MAILLARD, G. TARRAGO, N. LACOME,

G. POUSSIGUE, A. LEVY, AND G. GUELACHVILI 1987. High-resolution spectroscopy of Saturn at 5 μm. I. Observations and atmospheric composition. *Bull. Amer. Astron. Soc.* **19,** 848–849.

FEGLEY, M. B. 1988. The chemistry of arsine (AsH_3) in the deep atmospheres of Saturn and Jupiter. *Bull. Amer. Astron. Soc.* **20,** 879.

FEGLEY, M. B., AND R. G. PRINN 1985. Equilibrium and nonequilibrium chemistry of Saturn's atmosphere: Implications for the observability of PH_3, N_2, CO, and GeH_4. *Astrophys. J.* **299,** 1067–1078.

FEGLEY, M. B., AND R. G. PRINN 1988a. Chemical constraints on the water and total oxygen abundances in the deep atmosphere of Jupiter. *Astrophys. J.* **324,** 621–625.

FEGLEY, M. B., AND R. G. PRINN 1988b. The predicted abundances of deuterium-bearing gases in the atmospheres of Jupiter and Saturn. *Astrophys. J.* **326,** 490–508.

FINK, U., AND H. P. LARSON 1978. Deuterated methane observed on Saturn. *Science* **201,** 343–345.

FINK, U., H. P. LARSON, G. L. BJORAKER, AND J. R. JOHNSON 1983. The NH_3 spectrum in Saturn's 5 micron window. *Astrophys. J.* **268,** 880–888.

FINK, U., H. P. LARSON, AND R. R. TREFFERS 1978. Germane in the atmosphere of Jupiter. *Icarus* **34,** 344–354.

GAUTIER, D., AND T. OWEN 1989. The composition of outer planet atmospheres. In *Origin and Evolution of Planetary and Satellite Atmospheres* (S. K. Atreya, J. B. Pollack, and M. S. Matthews, Eds.), pp. 487–512. Univ. of Arizona Press, Tucson.

GIVER, L. P., AND C. CHACKERIAN 1990. *Intensity Measurements of Individual Lines and Manifolds in the Spectrum of the 5 Micron Fundamental Band of Germane.* Preprint.

HANEL, R., *et al.* 1981. Infrared observations of the Saturnian system from Voyager 1. *Science* **212,** 192–200.

LARSON, H. P., AND U. FINK 1975. Infrared Fourier spectrometer for laboratory use and for astronomical studies from aircraft and ground-based telescopes. *Appl. Opt.* **14,** 2085–2095.

LARSON, H. P., U. FINK, H. A. SMITH, AND D. S. DAVIS 1980. The middle-infrared spectrum of Saturn: Evidence for phosphine and upper limits to other trace atmospheric constituents. *Astrophys. J.* **240,** 327–337.

LARSON, H. P., R. R. TREFFERS, AND U. FINK 1977. Phosphine in Jupiter's atmosphere: The evidence from high-altitude observations at 5 micrometers. *Astrophys. J.* **211,** 972–979.

LELLOUCH, E., N. LACOME, G. GUELACHVILI, G. TARRAGO, AND T. ENCRENAZ 1987. Ammonia: Experimental absolute line strengths and self-broadening parameters in the 1800- to 2000-cm^{-1} range. *J. Mol. Spectrosc.* **124,** 333–347.

LEWIS, J. S., AND R. G. PRINN 1980. Kinetic inhibition of CO and N_2 reduction in the solar nebula. *Astrophys. J.* **238,** 357–364.

LUNINE, J. I., AND D. M. HUNTEN 1987. Moist convection and the abundances of water in the troposphere of Jupiter. *Icarus* **69,** 566–570.

MARTEN, A., R. COURTIN, D. GAUTIER, AND A. LACOMBE 1980. Ammonia vertical density profiles in Jupiter and Saturn from their radioelectric and infrared emissivities. *Icarus* **41,** 410–422.

NOLL, K. S. 1987. *Carbon monoxide and disequilibrium dynamics in Saturn and Jupiter.* Ph.D. thesis, State University of New York at Stony Brook.

NOLL, K. S., R. F. KNACKE, T. R. GEBALLE, AND A. T. TOKUNAGA 1986. Detection of carbon monoxide in Saturn. *Astrophys. J.* **309,** L91–L94.

NOLL, K. S., T. R. GEBALLE, AND R. F. KNACKE 1989. Arsine in Saturn and Jupiter. *Astrophys. J.* **338,** L71–L74.

NOLL, K. S., R. F. KNACKE, T. R. GEBALLE, AND A. T. TOKUNAGA 1988a. Evidence for germane in Saturn. *Icarus* **75,** 409–422.

NOLL, K. S., R. F. KNACKE, T. R. GEBALLE, AND A. T. TOKUNAGA 1988b. The origin and vertical distribution of carbon monoxide in Jupiter. *Astrophys. J.* **324,** 1210–1218.

NOLL, K. S., H. P. LARSON, AND T. R. GEBALLE 1990. The abundance of AsH_3 in Jupiter. *Icarus* **83,** 494–499.

OWEN, T., B. L. LUTZ, AND C. DE BERGH 1986. Deuterium in the outer solar system: Evidence for two distinct reservoirs. *Nature* **320,** 244–246.

POLLACK, J. B., AND P. BODENHEIMER 1989. Theories of the origin and evolution of the giant planets. In *Origin and Evolution of Planetary and Satellite Atmospheres* (S. K. Atreya, J. B. Pollack, and M. S. Matthews, Eds.), pp. 564–602. Univ. of Arizona Press, Tucson.

POLLACK, J. B., M. PODOLAK, P. BODENHEIMER, AND B. CHRISTOFFERSON 1986. Planetesimal dissolution in the envelopes of the forming, giant planets. *Icarus* **67,** 409–443.

PRATHER, M., J. LOGAN, AND M. MCELROY 1978. Carbon monoxide in Jupiter's upper atmosphere: An extraplanetary source. *Astrophys. J.* **223,** 1072–1081.

PRINN, R. G., AND S. S. BARSHAY 1977. Carbon monoxide on Jupiter and implications for atmospheric convection. *Science* **198,** 1031–1034.

PRINN, R. G., H. P. LARSON, J. J. CALDWELL, AND D. GAUTIER 1984. Composition and chemistry of Saturn's atmosphere. In *Saturn* (T. Gehrels and M. S. Matthews, Eds.), pp. 88–149. Univ. of Arizona Press, Tucson.

ROTHMAN, L. S., R. R. GAMACHE, A. BARBE, A. GOLDMAN, J. R. GILLIS, L. R. BROWN, R. A. TOTH, J.-M. FLAUD, AND C. CAMY-PEYRET 1983. AFGL atmospheric absorption line parameters compilation: 1982 edition. *Appl. Opt.* **22,** 2247–2256.

SIMONELLI, D. P., J. B. POLLACK, C. P. MCKAY, R. T. REYNOLDS, AND A. L. SUMMERS 1989. The carbon budget in the outer solar nebula. *Icarus* **82,** 1–35.

TARRAGO, G., N. LACOME, G. POUSSIGUE, A. LEVY, AND G. GUELACHVILI 1987. Communications FB5 and FB6. 42nd Symposium on Molecular Spectroscopy. Columbus, OH.

TOKUNAGA, A. T., H. L. DINERSTEIN, D. F. LESTER, AND D. M. RANK 1980. The phosphine abundance on Saturn derived from new 10 micrometer spectra. *Icarus* **42,** 79–85. Erratum. *Icarus* **48,** 540, 1981.

TOMASKO, M. G., R. A. WEST, G. S. ORTON, AND V. G. TEJFEL 1984. Clouds and aerosols in Saturn's atmosphere. In *Saturn* (T. Gehrels and M. S. Matthews, Eds.), pp. 150–194. Univ. of Arizona Press, Tucson.

TREFFERS, R. R., H. P. LARSON, U. FINK, AND T. N. GAUTIER 1978. Upper limits to trace constituents in Jupiter's atmosphere from an analysis of its 5-μ spectrum. *Icarus* **34,** 331–343.

VARANASI, P., AND S. CHUDAMANI 1987. Intensities and H_2-broadened half-widths of germane lines around 4.7 μm at temperatures relevant to Jupiter's atmosphere. *J. Quant. Spectrosc. Radiat. Transfer* **38,** 173–177.